RSC Sustainability

ROYAL SOCIETY OF CHEMISTRY

TUTORIAL REVIEW

View Article Online
View Journal | View Issue

Cite this: *RSC Sustainability*, 2025, **3**, 5089

Preparation methods of $V^{3.5+}$ electrolyte and related capacity recovery strategies for vanadium flow batteries: a review

Pai Wang,[ab] Yu Qin,*[c] Lina Wang,[ab] Tao Qi[a] and Fancheng Meng *[ab]

Vanadium flow batteries (VFBs) represent a prominent large-scale long-duration energy storage technology, with vanadium electrolyte serving as a critical component that fundamentally governs battery performance. In practical implementations, mixed-valence $V^{3.5+}$ electrolyte is universally employed as the initial active solution in both half-cells. The preparation methodology and raw material selection for $V^{3.5+}$ electrolyte substantially influence both the economic viability and environmental sustainability of VFB systems. This review systematically examines established techniques for preparing $V^{3.5+}$ electrolyte, including the chemical reduction method, electrolysis method, and chemical reduction–electrolysis method, and further classifies them systematically, analyzes the basic principles, process architecture, key equipment, technical advantages and existing problems of each process, and discusses the potential of each method in sustainable application. In addition, this study also analyzed the capacity attenuation mechanism of vanadium batteries, and summarized the capacity recovery strategies. The reduction process of high valence vanadium ions involved in the capacity recovery process and the preparation of $V^{3.5+}$ electrolyte have high commonality in chemical principle and process technology. The review concludes with a forward-looking perspective on technological innovations in electrolyte synthesis, emphasizing sustainable production routes and performance optimization strategies for next-generation VFB applications.

Received 30th June 2025
Accepted 21st September 2025

DOI: 10.1039/d5su00532a

rsc.li/rscsus

[a]*National Engineering Research Center of Green Recycling for Strategic Metal Resources, Institute of Process Engineering, Chinese Academy of Sciences, No. 1, North 2nd Street, Zhongguancun, Haidian District, Beijing 100190, China. E-mail: fcmeng@ipe.ac.cn; Tel: +86-10-82544848*

[b]*School of Chemical Engineering, University of Chinese Academy of Sciences, Beijing 101408, China*

[c]*Shenyang Hengjiu Antai Environmental Protection and Energy Conservation Technology Co., Ltd, No. 158, Puhe Road, Shenbei New District, Shenyang 110127, Liaoning Province, China. E-mail: qiny@h9at.com; Tel: +86-24-85635968*

Pai Wang

Pai Wang received a bachelor's degree in environmental engineering from Yanshan University, China. She is now a master's student at the Institute of Process Engineering, Chinese Academy of Sciences. Her research focuses on the preparation process (VFB) of electrolyte for 3.5-valent vanadium flow batteries, aiming at overcoming the technical bottleneck of the core material vanadium electrolyte in terms of cost, concentration and purity.

Yu Qin

Yu Qin serves as the Deputy General Manager and Director of the Research Institute at Shenyang Hengjiu Antai Environmental Protection and Energy Conservation Technology Co., Ltd. He has led his team in developing new technologies in vanadium flow batteries, solid thermal energy storage, water-based thermal energy storage/cooling, phase change thermal energy storage (PCMS), and high-voltage electrode boilers. His research covers core components in the vanadium flow battery energy storage system, including membranes, stacks, electrolytes, and system integration.

Sustainability spotlight

Vanadium flow batteries (VFBs) are vital for integrating renewable energy and enabling grid decarbonization. However, the economic and environmental costs of preparing essential $V^{3.5+}$ electrolytes pose significant barriers to sustainable VFB deployment. This review critically analyzes $V^{3.5+}$ electrolyte synthesis methods, highlighting pathways to reduce resource consumption, minimize waste, and lower production energy intensity. By advancing efficient, low-impact electrolyte manufacturing and capacity restoration techniques, this work directly contributes to making large-scale, long-duration energy storage more affordable and environmentally sound. These advancements align with key UN Sustainable Development Goals: SDG 7 (Affordable and Clean Energy) by enabling renewable storage, SDG 9 (Industry, Innovation and Infrastructure) through cleaner production innovation, and SDG 12 (Responsible Consumption and Production) by promoting resource efficiency and waste reduction in battery value chains.

1 Introduction

Renewable energy sources are receiving widespread attention because the existing fossil fuel-based energy infrastructure cannot meet the requirements of sustainable social development.[1,2] The VFB stands out as a mature large-scale energy storage technology,[3–5] which is recognized as one of the most advanced energy storage technologies today; it offers advantages such as long cycle life, flexible design, and safe system operation.[6–8] Pioneered by the University of New South Wales in the 1980s,[9,10] the VFB achieves mutual conversion between chemical energy and electrical energy through reversible changes in the valence states of vanadium ions in sulfuric acid electrolyte: during charging, electrical energy is converted into chemical energy for storage, while during discharging, chemical energy is reconverted into electrical energy for output. Its energy storage principle and energy conversion during the charge–discharge process are shown in Fig. 1. This unique single-element design eliminates cross-contamination through membrane infiltration theoretically.[11] When the battery is charged, the anode undergoes an oxidation reaction, and V^{4+} loses electrons and is oxidized to V^{5+}. At the same time, a reduction reaction occurs at the negative electrode, and V^{3+} gains electrons and is reduced to V^{2+}. These electrons flow through an external circuit to charge the battery. During the whole charging and discharging process, H^+ ions in the positive and negative solutions migrate through the proton exchange membrane to maintain the charge balance.[12] The reaction equations for the discharging process are shown by eqn (1)–(3)[13,14] while the charge process is the reverse of these reactions:

Positive:

$$VO_2^+ + 2H^+ + e^- \rightarrow VO^{2+} + H_2O \; E_0 = 1.00 \text{ V} \quad (1)$$

Negative:

$$V^{2+} \rightarrow V^{3+} + e^- \; E_0 = -0.25 \text{ V} \quad (2)$$

Net:

$$VO_2^+ + 2H^+ + V^{2+} \rightarrow VO^{2+} + V^{3+} + H_2O \; E_0 = 1.25 \text{ V} \quad (3)$$

As the energy carrier of VFBs, the vanadium electrolyte is one of the key materials and its performance and quality are key to the safe operation of VFBs over a long period of time.[16] The $V^{3.5+}$ electrolyte refers to an electrolyte in which the average valence state of vanadium ions is 3.5, meaning it is an equimolar mixture of V^{4+} and V^{3+} ions as the initial valence states for the positive and negative electrolytes.[17] The $V^{3.5+}$ electrolyte, as the initial electrolyte, exhibits symmetric valence state changes, and the transfer of electrons and ions during the reaction process is mutually balanced, thus eliminating the need for additional adjustments to the positive and negative electrode capacities. The preparation of vanadium electrolyte involves the conversion of different valence vanadium ions, and vanadium electrolyte is usually prepared with high-purity V_2O_5 (purity > 99.5%) as the raw material[18,19] The amount of electrolyte can even reach hundreds of tons in the megawatt VFB system, and the cost of vanadium electrolyte generally accounts for more than 50% of the total cost of VFB energy storage systems.[12] Generally, the cost of vanadium electrolyte is determined by the raw materials and preparation methods.[20,21] Besides, the long-term operational challenges of VFBs primarily stem from electrolyte concentration decay, volume changes and valence state imbalances,[22,23] which collectively contribute to capacity fading over time.[24–27] The adjustment of the valence state of vanadium ions, the recovery of electrolyte capacity and recycling are key to realizing the economy and sustainability of the VFB storage system.

In this review, we systematically present the classification and critical evaluation of modern methodologies employed in the preparation of $V^{3.5+}$ electrolyte. A comprehensive review of the primary synthesis techniques such as the chemical reduction method, electrolysis method, chemical reduction–electrolysis method is conducted. Special attention is given to the

Fancheng Meng

Fancheng Meng is an Associate Professor and Master's Supervisor at the Institute of Process Engineering, Chinese Academy of Sciences. His expertise and research interests include hydrometallurgy, solvent extraction separation, process design and simulation, solution thermodynamics, and quantum chemistry calculations. He has published over 30 peer-reviewed journal papers in these fields. Currently, he leads several research projects and continues to investigate the preparation of electrolytes for vanadium flow batteries via the solvent extraction method from various vanadium feedstocks.

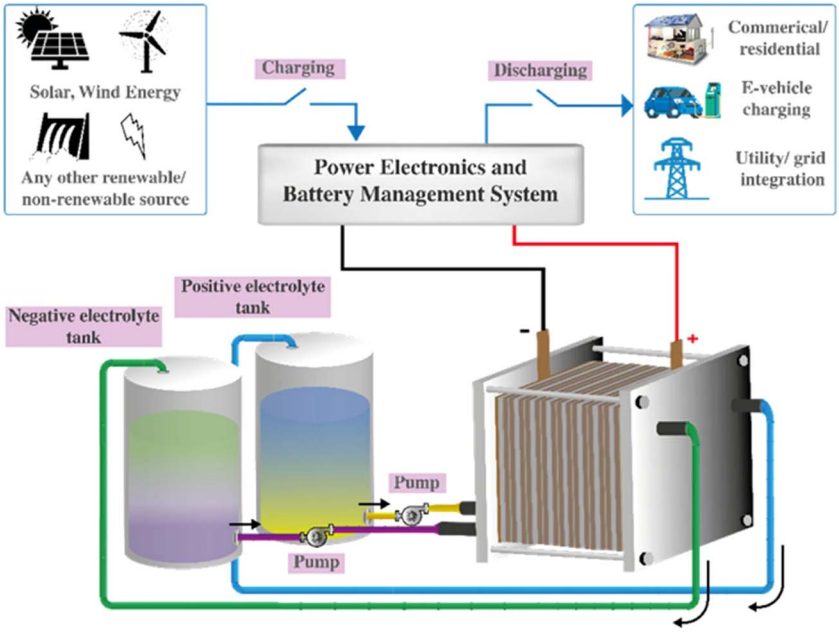

Fig. 1 VFB energy storage schematic[15] (reprinted with permission from Springer Nature).

Table 1 Stability of V^{n+} sulfate solutions[28]

V^{n+} species	V^{n+}, M	Total sulfate, M	T, °C	Time
V^{3+}	2.0	5.0	−5	Stable (>10 d)
	2.0	5.0	25	Stable (>10 d)
	2.0	5.0	40	Stable (>10 d)
$V^{4+}(VO^{2+})$	2.0	5.0	−5	18 h
	2.0	5.0	25	95 h
	2.0	5.0	40	Stable (>10 d)

selection of vanadium precursors and valence state manipulation. Furthermore, this review addresses the capacity fading issues while providing a comprehensive summary of capacity restoration strategies for vanadium electrolytes.

2 Chemical properties of $V^{3.5+}$ electrolyte

2.1 $V^{3.5+}$ electrolyte composition and stability

In practical application, there are detailed requirements for the concentration of vanadium ions and sulfuric acid in $V^{3.5+}$ electrolyte, and the requirements for impurity elements are more stringent. V^{2+} ions are unstable and prone to oxidation reactions, while V^{5+} ions tend to form precipitates. In contrast, V^{3+} and V^{4+} ions are relatively stable, with stability data shown in Table 1. This is one of the main reasons why vanadium electrolyte is prepared, stored, transported and initially used in the form of $V^{3.5+}$ electrolyte.

$V^{3.5+}$ electrolytes typically utilize sulfuric acid as the primary supporting electrolyte, with sulfate ions acting as the coordinating ligands. The common composition of the electrolyte consists of vanadium ion concentrations ranging from 1.5 to 1.8 mol L^{-1} and sulfate ion concentrations between 4 and 5 mol L^{-1} as shown in Table 2. The dual functionality of H_2SO_4 as both a proton donor and a coordinating medium enhances the stability and ionic conductivity of the electrolyte. Chloride and phosphate ions inhibit vanadium ion aggregation through competitive coordination, thereby inhibiting aggregation and enhancing colloidal stability and the reversibility of redox reactions; thus HCl and mixed acids such as H_2SO_4–HCl and H_2SO_4–H_3PO_4 are used as the supporting electrolytes with typical compositions featuring 1.5–2 M vanadium ions in a total acid concentration of 4–5 M. The introduction of HCl electrolyte can improve the solubility of vanadium ions and the thermal stability of electrolyte, but there is a great risk of chlorine leakage and equipment corrosion in actual use. Optimizing the electrolyte concentration within different acid systems can significantly improve the temperature adaptability and energy density of VFBs.

Table 2 Composition of vanadium electrolytes in different systems

	V, M	Sulfate ions, M	HCl, M	H_3PO_4, M
H_2SO_4	1.5–2.0	4.0–5.0	—	—
HCl[29,30]	1.5–2.5	—	5.0–6.0	—
H_2SO_4 + HCl[31,32]	2.5–3.0	2.0–3.0	5.5–6.5	—
H_2SO_4 + H_3PO_4 (ref. 33)	1.5–2.0	3.0–3.5	—	0.1–1.0

2.2 Solvation structures of vanadium ions in $V^{3.5+}$ electrolytes

Vanadium ions exhibit complex speciation in aqueous solutions, with its oxidation states and stability highly dependent on pH and electrode potential as shown in Fig. 2. Under acidic conditions, vanadium can exist in four ionic forms, including

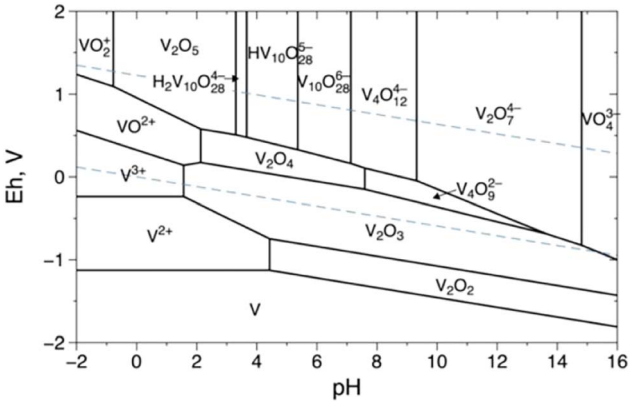

Fig. 2 Eh–pH diagram for vanadium species at [V] = 1 M (ref. 34) (reprinted with permission from American Chemical Society).

V^{2+}, V^{3+}, VO^{2+}, and VO_2^+. The dominant ions at low potentials are V^{3+} and VO^{2+}, whereas when the potential exceeds approximately 0.8 V, the dominant ions shift to VO^{2+} and VO_2^+.This indicates that in strongly acidic solutions of $V^{3.5+}$ electrolyte, vanadium ions primarily exist in the forms of VO^{2+} and V^{3+}.

As for $V^{3.5+}$ electrolyte, the most stable configurations formed by V^{3+} and V^{4+} ions in different acid solutions are presented in Fig. 3. It shows that V^{3+} ions form hexahydrate structures with an octahedral geometry denoted as $[V(H_2O)_6]^{3+}$.[35–37] The VO^{2+} ion adopts a pentahydrate structure, forming an octahedral geometry with one vanadyl oxygen and five water molecules represented as $[VO(H_2O)_5]^{2+}$.[38–43] These structures highlight the influence of charge density and oxidation state on the coordination chemistry of vanadium ions.

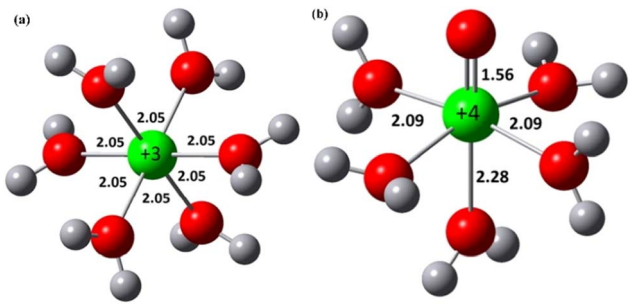

Fig. 3 Structures of (a) V^{3+} and (b) V^{4+} ions and their first solvation shell water molecules by DFT[44] (reprinted with permission from Elsevier).

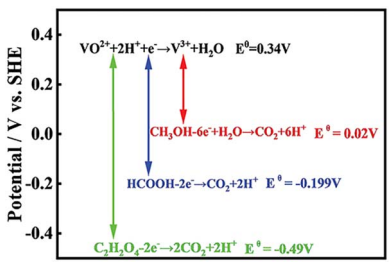

Fig. 4 Redox potential of V^{4+}/V^{3+} (ref. 52) (reprinted with permission from MDPI).

2.3 Basic redox reactions of preparing $V^{3.5+}$ electrolyte

The preparation of $V^{3.5+}$ electrolyte from pentavalent vanadium is essentially a step-by-step reduction process: first, V^{5+} is reduced to V^{4+}, and then V^{4+} is further reduced to V^{3+}. The conventional method is to dissolve V_2O_5 in sulfuric acid aqueous solution and use oxalic acid,[45–47] acetic acid,[48] sulfur dioxide[49] or glycerol[50] as reducing agents to prepare $V^{3.5+}$ electrolyte.[51] However, these traditional reductants can only realize the transformation from V^{5+} into V^{4+} in the water phase environment, and cannot continue to reduce V^{4+} to V^{3+} due to their reducing ability. Therefore, the realization of efficient and deep reduction of V^{4+} to V^{3+} has become the key to prepare $V^{3.5+}$ balanced electrolyte from pentavalent vanadium compounds such as V_2O_5.

The redox behavior of vanadium ions in different oxidation states is illustrated by reduction reactions as reflected by their standard electrode potentials (E_0). From the point of view of standard electrode potential, whether the reduction reaction from V^{4+} to V^{3+} in eqn (4) can be carried out mainly depends on whether the oxidation potential of the reducing agent is greater than the reduction potential by 0.34 V.[52] As shown in Fig. 4, CH_3OH, HCOOH and $C_2H_2O_4$ show redox potentials lower than those of V^{4+}/V^{3+} pairs and $C_2H_2O_4$ (0.83 V) > HCOOH (0.54 V) > CH_3OH (0.32 V). Thermodynamically, oxalic acid can further reduce V^{4+} to V^{3+}, but the reaction rate constant of V reduction by oxalic acid is very low and the energy barrier is very high, so the reaction is extremely slow; so it is difficult for the process of converting V^{4+} to V^{3+} to occur. Compared with formic acid, its oxidation potential provides sufficient thermodynamic driving force, and its more direct oxidation path and faster reaction kinetics enable it to effectively overcome the energy barrier and realize the reduction from V^{4+} to V^{3+}.

$$VO^{2+} + 2H^+ + e^- \rightarrow V^{3+} + H_2O \; E_0 = 0.34 \text{ V} \quad (4)$$

2.4 Selection of vanadium raw materials

Vanadium is generally extracted from ores such as titanomagnetite[53] and stone coal mine through high-temperature roasting techniques,[54,55] which results in the production of V_2O_5, which is the main raw material for the preparation of electrolytes for VFBs.[56,57] Vanadium ore is typically processed through roasting followed by either acid or alkali leaching. The dissolved vanadium is then enriched and precipitated to yield crude ammonium metavanadate, and industrial ammonium metavanadate (purity 90–95%) is purified to over 99.5% by extraction, ion exchange resin or other processes to obtain high-purity ammonium metavanadate.[58] As a precursor of high-purity V_2O_5, the cost core of high-purity ammonium metavanadate lies in the grade of raw vanadium ore and waste and the accuracy of impurity control.

The preparation of $V^{3.5+}$ electrolyte mostly uses high-purity V_2O_5 as the raw material to meet its purity and stability requirements, and its supply chain is mature and widely used. Using V_2O_5 as the raw material, V^{5+} is first reduced to V^{4+} by the chemical reduction–electrolysis method, and V^{4+} electrolyte is electrolyzed to 3.5 valence, or V_2O_5 slurry is directly electrolyzed

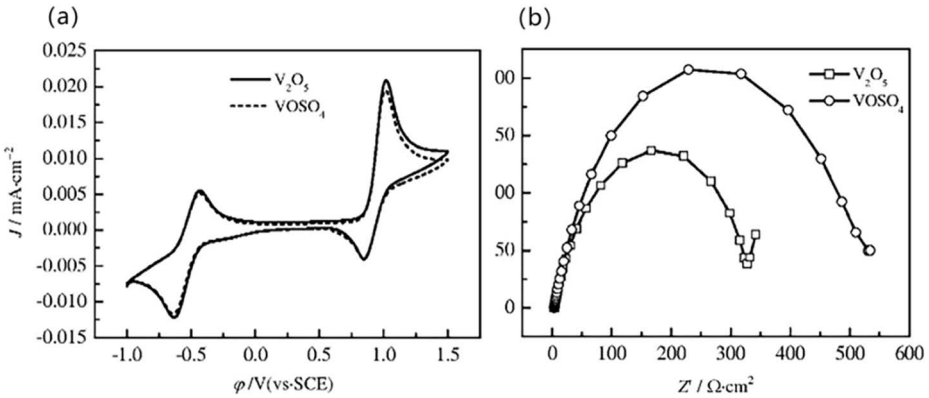

Fig. 5 (a) CV; (b) impedance spectrum of V^{3+} electrolytes prepared with different raw materials[59] (reprinted with permission from MDPI).

to 3.5 valence. At present, this has turned out to be a diversified raw material strategy. For instance, high-purity ammonium metavanadate can be used as a direct raw material to prepare $V^{3.5+}$ electrolyte by solid-phase reduction roasting and acid dissolution and the solvent extraction–electrolysis method with vanadium leaching solution or vanadium slag as raw materials.

As shown in Fig. 5(a), the cyclic voltammetry (CV) curves of vanadium electrolytes prepared from high-purity V_2O_5 and impurity-containing $VOSO_4$ are basically the same, indicating that they have similar electrochemical activities. However, as can be seen from the impedance spectrum in Fig. 5(b), the smaller impedance arc of the V_2O_5 curve shows that the resistance of the electrolyte at the electrode interface is smaller and the reaction is faster, which is due to its extremely low impurity content, thus ensuring the performance of the electrolyte in long-term use.[59] This difference is mainly due to the extremely low impurity content of high-purity V_2O_5 raw materials, which significantly improves the

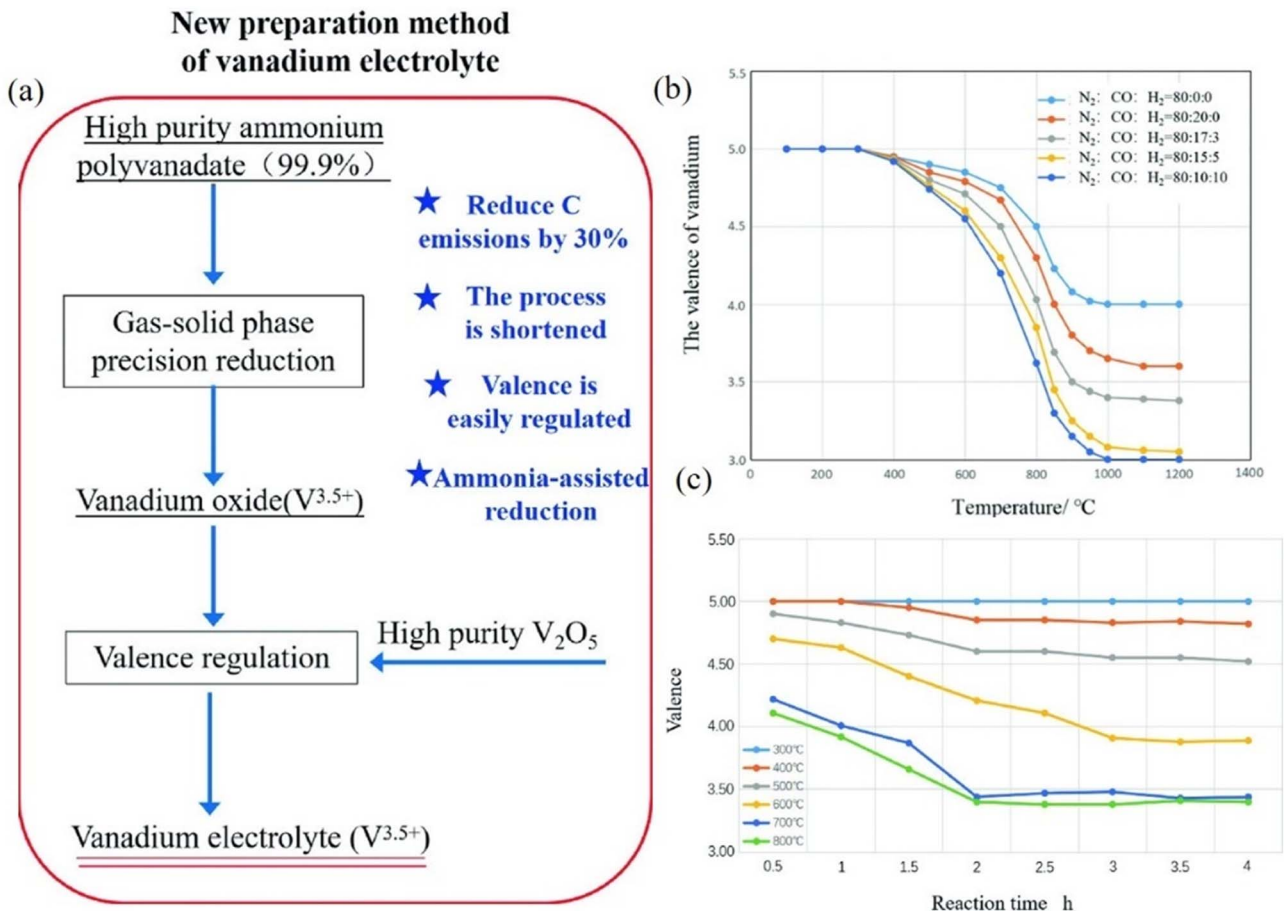

Fig. 6 (a) Process flow; the influence of (b) different reducing agent partial pressures; (c) temperature and reduction time[66] (reprinted with permission from Springer Nature).

interface performance and long-term operation stability of electrolyte. In practical application, high-purity V_2O_5 has been widely used on the industrial scale because of its mature process and industrial chain. At present, the industrial supply of high-purity $VOSO_4$ is limited and the output is small. The above results also reflect the influence of raw material purity on the electrochemical performance of vanadium electrolyte.

3 Preparation methods of $V^{3.5+}$ electrolyte

The most direct preparation method of $V^{3.5+}$ electrolyte is to use high-purity $VOSO_4$ and $V_2(SO_4)_3$ or V_2O_3, V_2O_5, VCl_3, *etc.* as raw materials,[60] mix them by using a valence ratio of 3.5 and dissolve them in sulfuric acid or hydrochloric acid.[61,62] However, the requirement of high purity of vanadium raw materials and poor solubility of vanadium oxides have made the acid dissolution method seldom used alone in practical applications. At present, the methods of preparing $V^{3.5+}$ electrolyte can be mainly divided into the chemical reduction method, electrolysis method and chemical reduction–electrolysis method, among which the chemical reduction–electrolysis method has become the mainstream method of industrial production of $V^{3.5+}$ electrolyte. The following is a detailed overview of its basic processes.

3.1 Chemical reduction method

3.1.1 Solid-phase reduction-acid dissolution method. Solid-phase reduction-acid dissolution is a method for preparing vanadium oxides by solid-phase reduction and then dissolving them in acid to obtain a $V^{3.5+}$ electrolyte,[63,64] in which the vanadium raw material provides the active substance of VFBs, and the reducing agent regulates the valence of the vanadium electrolyte. To promote the reduction of vanadium from V^{4+} to V^{3+} oxidation states, it usually requires the use of strong reducing agents, such as hydrogen gas[65] and hydrazine hydrate at elevated temperatures.

Wu *et al.*[66] developed a short-process ammonium salt vapor reduction method using ammonium metavanadate or polyvanadate as vanadium sources as presented in Fig. 6(a) and using V_2O_5 as the raw material, under the conditions of a reducing atmosphere of $N_2 : CO{:}H_2 = 80 : 17 : 3$ and reaction at 700 °C and 2 h as shown in Fig. 6(b) and eqn (5)–(7). It is carried out by controlled reduction to generate mixed valence oxide containing VO_2 and V_2O_3. The V^{4+}/V^{3+} ratio may not be exactly 1 : 1 due to process fluctuation; it is necessary to add high-purity V_2O_5 to adjust the valence state to 3.5. When V_2O_5 reacts with V^{3+} in acidic solution, a redox reaction occurs as shown in eqn (8). V^{3+} acts as a chemical reducing agent that significantly accelerates the dissolution of V_2O_5, thereby mitigating its poor solubility. Although its solubility is low, the redox reaction will increase its solubility under the conditions of heating and stirring, and the valence state can be fine-tuned and stabilized by controlling its addition amount. Vanadium oxides have a stable crystal structure, high lattice energy and generally poor solubility; most dissolution processes control acid concentration and reaction conditions according to the valence state of vanadium, such as temperature and pressure, or destroy the crystal lattice through the synergistic effect of acid dissolution and reduction.

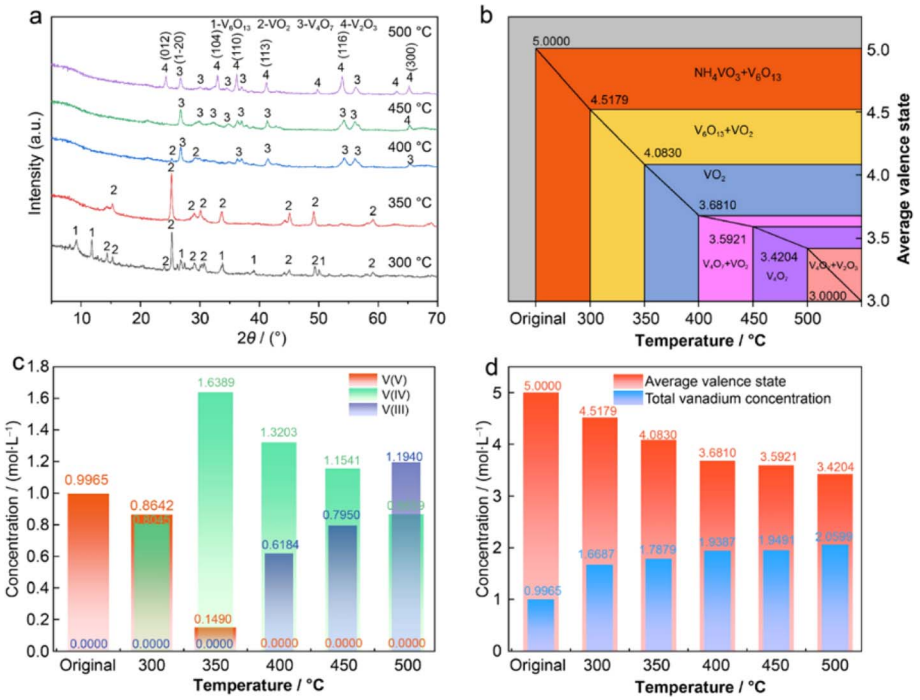

Fig. 7 At different temperatures: (a) XRD; (b) the average valence state and phase change; (c) the concentration of vanadium; (d) the variation of total vanadium concentration and average valence state[67] (reprinted with permission from Springer Nature).

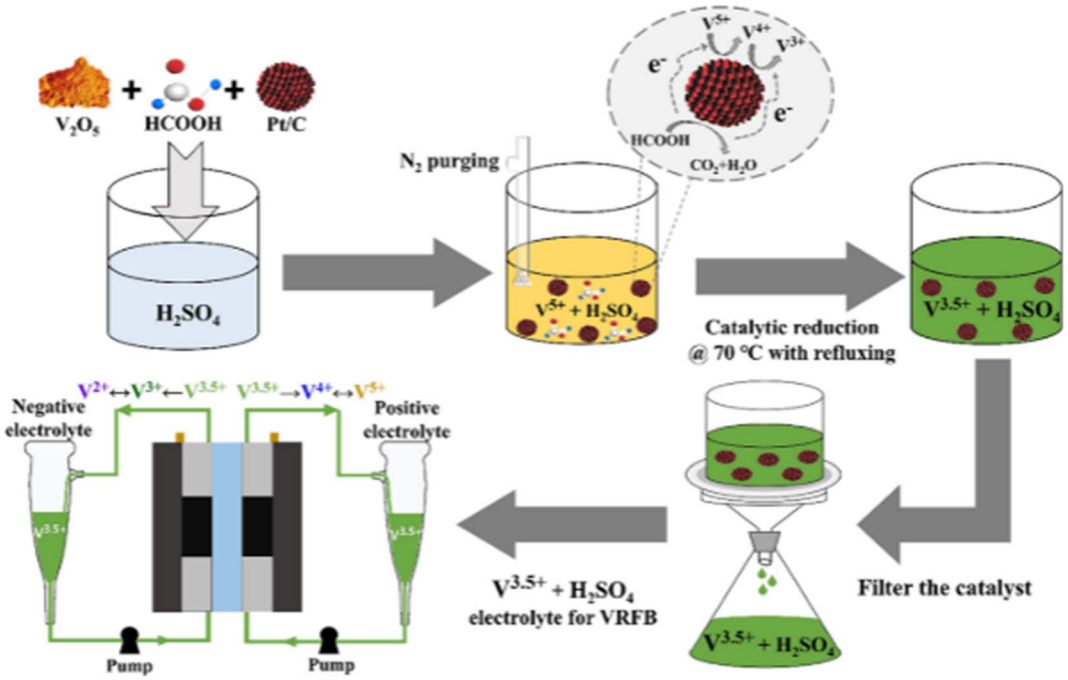

Fig. 8 Schematic of $V^{3.5+}$ electrolyte preparation using hydrothermal reduction[16] (reprinted with permission from American Chemical Society).

$$(NH_4)_2V_6O_{16} \rightarrow 6VO_2 + N_2 + 4H_2O \quad (5)$$

$$(NH_4)_2V_6O_{16} + 3CO \rightarrow 3V_2O_3 + 3CO_2 + N_2 + 4H_2O \quad (6)$$

$$(NH_4)_2V_6O_{16} + 3H_2 \rightarrow 3V_2O_3 + N_2 + 7H_2O \quad (7)$$

$$V_2O_5 + 2V^{3+} + 2H^+ \rightarrow 4VO^{2+} + H_2O \quad (8)$$

Du *et al.*[67] provided an approach for preparing $V^{3.5+}$ electrolyte with a short process. Using ammonia metavanadate as the raw material and ammonia as the reducing agent, the temperature is increased to 400–500 °C and when the temperature reaches the reaction temperature, ammonia gas is introduced for the reduction reaction and the obtained roasted reduction product is acid-dissolved from a tube furnace to obtain vanadium electrolyte. The different valence states of vanadium in the reduction process are shown in Fig. 7(a–c), and NH_4VO_3 in the raw material only contains V^{5+}. With the increase in reduction temperature, the concentration of V^{5+} gradually decreased and V^{4+} appeared and its concentration began to increase. At 350–400 °C, the product began to transform from V^{4+} into V^{3+}. In the whole reduction process, the total average valence state of vanadium decreased in turn, indicating that the valence state of vanadium in the product was continuously reduced. In the reduction process as shown in Fig. 7(d), V_4O_7 can be obtained at 400–500 °C. $V^{3.5+}$ electrolyte can be obtained after acid dissolution, and it is found that increasing the reaction temperature and ammonia flow rate and prolonging the reaction time are conducive to the reduction process; this method provides a short process to prepare a $V^{3.5+}$ electrolyte.

In summary, the solid-state reduction-acid dissolution method is used to prepare low-valent vanadium oxide through high-temperature reduction, and the acid dissolution of vanadium oxide is promoted through oxidation and reduction of V^{3+} and V^{5+}. The process flow is relatively simple, and the use of gases such as hydrogen can avoid the problem of reducing agent residue. However, it is necessary to accurately control the high-temperature reducing atmosphere, which involves flammable and explosive gases such as H_2, and has high energy consumption and high safety requirements for equipment.

3.1.2 Catalytic reduction method. The catalytic reduction method is used for the preparation of $V^{3.5+}$ electrolyte by chemical reduction under the action of catalysts, and the key to its application lies in the selection of catalysts and reducing agents. As the reducing agent of V^{4+} solution, methanol, formic acid and oxalic acid are usually chosen, which have lower cost and lower standard redox potential and the oxidation products are H_2O and CO_2 which are cleaner. For the choice of catalyst, the Pt/C catalyst is widely used in catalytic reduction due to its high activity. The reactors used include the one-pot reactor, column reactor, fixed-bed reactor and fuel cell type reactor.

3.1.2.1 One-pot reactor. A one-pot reactor is a relatively simple reaction mode. At a temperature of 70 °C in a N_2 atmosphere, V_2O_5, formic acid and Pt/C are mixed for a hydrothermal reaction with formic acid as the reducing agent and Pt/C as the catalyst.[16] The process flow for the preparation of $V^{3.5+}$ electrolyte using V_2O_5 as the feedstock is presented in Fig. 8, and the reaction equation is in eqn (9):

$$V_2O_5 + 3/2HCOOH + 5H^+ \rightarrow 2V^{3.5+}(VO^{2+} + V^{3+}) + 3/2CO_2 + 4H_2O \quad (9)$$

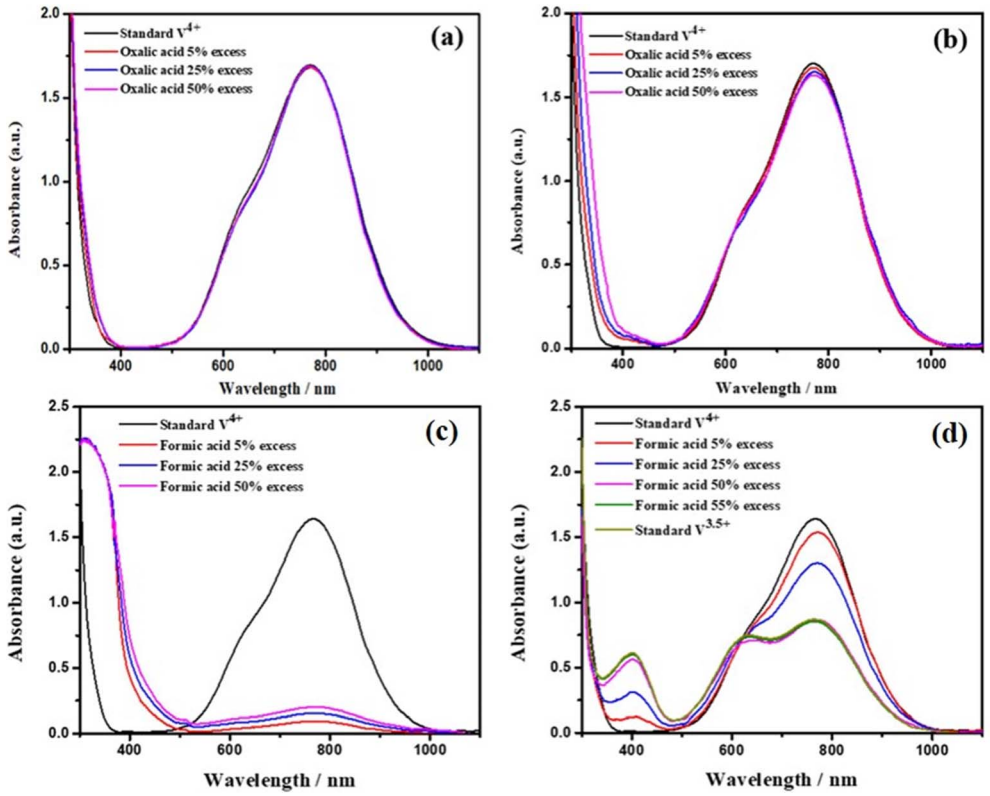

Fig. 9 UV-vis spectra of the electrolyte with (a) oxalic acid; (b) oxalic acid in the presence of a Pt/C catalyst; (c) formic acid; (d) formic acid in the presence of a Pt/C catalyst[16] (reprinted with permission from American Chemical Society).

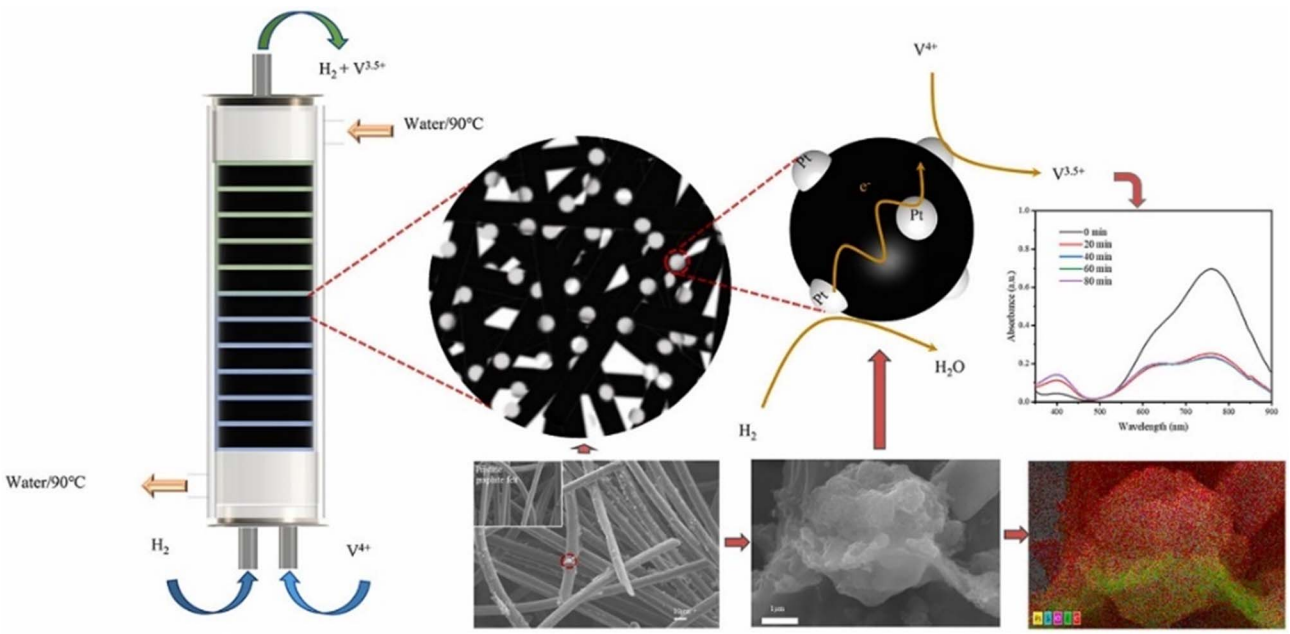

Fig. 10 Design model diagram of the column reactor[68] (reprinted with permission from Elsevier).

By analyzing the solution after catalytic reduction, the reduction effect and reaction process can be investigated. Potentiometric titration and UV-vis methods are often used to determine the concentration of vanadium ions in acidic systems. If oxalic acid and formic acid are used as reducing agents, as shown in Fig. 9(a and b), the UV-vis spectrum is compared with that of the standard vanadium solution. It was found that the UV-vis spectra of electrolyte solutions with excess

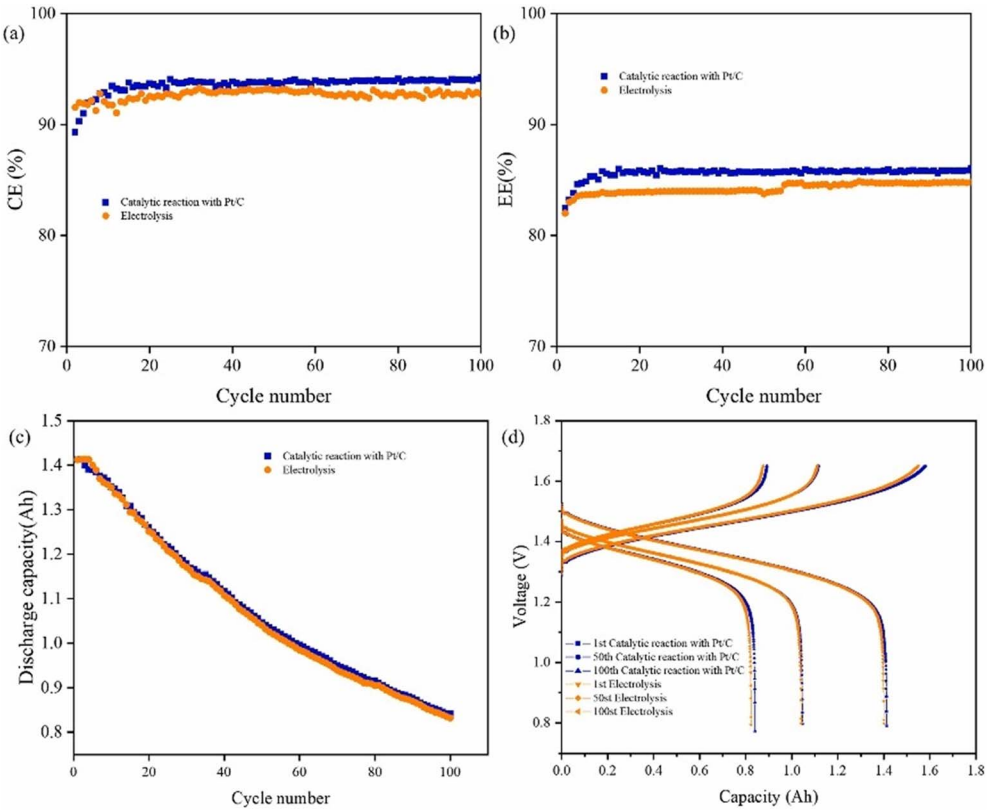

Fig. 11 (a) CE; (b) EE; (c) discharge capacities; (d) charge/discharge curves (reprinted with permission from Elsevier).

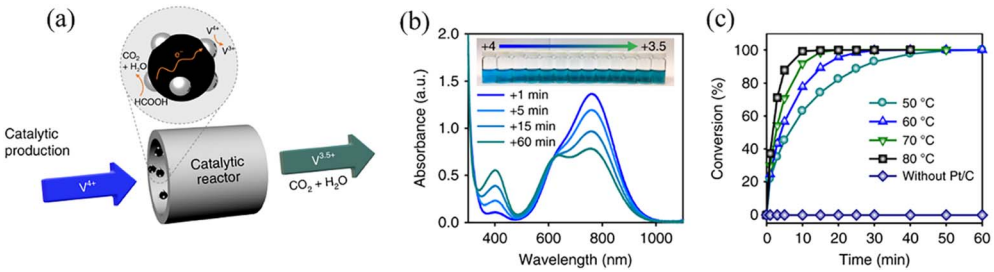

Fig. 12 (a) Reactor with fixed-bed Pt/C catalysts; (b) UV-vis spectra of the reactant electrolyte at different reaction times at 50 °C; (c) conversion diagram with and without Pt/C at 80 °C (ref. 17) (reprinted with permission from MDPI).

oxalic acid were almost the same as those of standard V^{4+} solution, and there was no characteristic V^{3+} peak, regardless of the presence of the Pt/C catalyst. As shown in Fig. 9(c and d), V^{5+} was partially reduced to V^{4+} in different excess formic acid solutions. When the Pt/C catalyst was introduced, a characteristic peak of V^{3+} appeared, and formic acid successfully reduced V^{5+} to $V^{3.5+}$. It was found that oxalic acid could not reduce V^{5+} to $V^{3.5+}$ even in the presence of the catalyst, but the use of formic acid could convert V^{5+} to $V^{3.5+}$. The oxidation state of the electrolyte was precisely controlled by adjusting the amount of formic acid, enabling the successful synthesis of $V^{3.5+}$ electrolytes.

3.1.2.2 Fixed bed reactor. The application of a column-type hydrothermal reactor is shown in Fig. 10, Xu *et al.*[68] proposed a method for the preparation of impurity-free $V^{3.5+}$ electrolyte by catalytic reduction using clean hydrogen, using the hydrothermal hydrogen reduction technique, and designed a Pt/C-modified graphite felt column-type catalytic reactor, with H_2 and $VOSO_4$ solution passed at the bottom of the reactor, and the $V^{3.5+}$ electrolyte obtained at the top. The reaction equation is in eqn (10):

$$2VOSO_4 + H_2 + H_2SO_4 \rightarrow V_2(SO_4)_3 + 2H_2O \quad (10)$$

Comparing the electrochemical properties of $V^{3.5+}$ electrolyte prepared by electrolysis and catalytic hydrogen reduction, the CE and EE curves in Fig. 11(a and b) are basically the same, and the discharge capacity is 59.5% as shown in Fig. 11(c), showing similar capacity attenuation. Fig. 11(d) further shows that the charge and discharge curves of the two electrolytes are almost

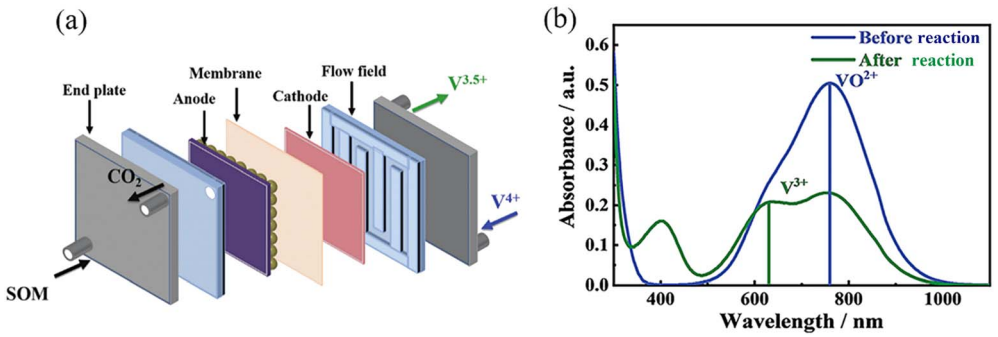

Fig. 13 (a) Schematic diagram and reaction mechanism of the fuel cell reactor; (b) UV-vis spectra of the electrolytes before and after the reaction[52] (reprinted with permission from MDPI).

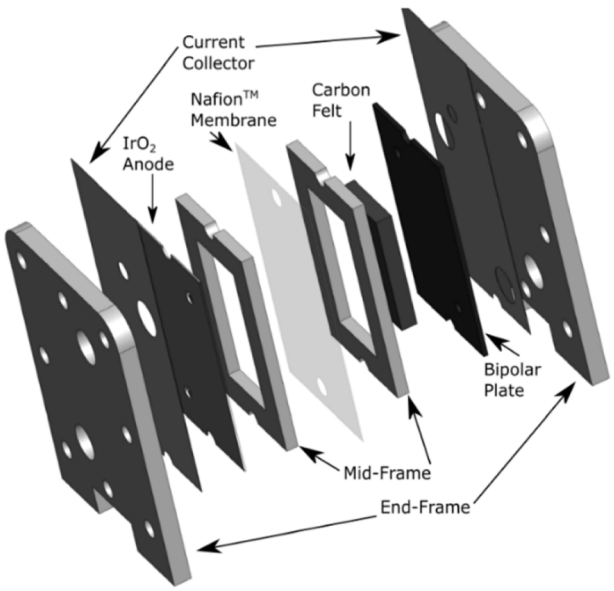

Fig. 14 Schematic diagram of the battery structure used in oxygen evolution electrolysis[72] (reprinted with permission from John Wiley and Sons).

the same at the 1st, 50th and 100th cycles. These results confirm that the electrochemical performance of electrolyte produced by catalytic hydrogen reduction is consistent with that of conventional electrolysis and meets the quality standards required for application. The use of hydrogen as the reducing agent in this catalytic reaction is cleaner and has no impurity residue, and the use of a Pt-based catalyst promotes the reduction of V^{4+} to V^{3+}, but this catalytic reactor requires a large amount of catalyst and has a high cost, and the use of hydrogen as the reducing agent also leads to transportation difficulties and safety hazards.

Another typical example of a fixed-bed type reactor is shown in Fig. 12(a). Heo *et al.*[17] constructed a fixed-bed flow catalyst reactor by stacking Pt/C-modified carbon felt. After V^{4+} electrolyte and formic acid pass through the catalytic reactor, they are converted into $V^{3.5+}$ and generate CO_2 and H_2O under the catalysis of Pt/C on the reactor wall.[37,69] As shown in the UV-vis spectrum in Fig. 12(b), the absorbance at the characteristic peak of V^{4+} decreased at 760 nm, while the absorbance at the characteristic peak of V^{3+} increased at 401 nm, indicating the transformation from V^{4+} into V^{3+}. As shown in Fig. 12(c), the reaction can hardly occur without the catalysis of Pt/C, and the reaction conversion rate increases with the increase in temperature at 50–80 °C, which shows that the presence of Pt/C and certain temperature conditions are essential for the chemical production of $V^{3.5+}$. It is very important to reduce the activation energy of formic acid oxidation, which proves the feasibility of continuous electrolyte production.

3.1.2.3 Fuel cell type reactor. As shown in Fig. 13(a), Sun *et al.*[52] constructed a bifunctional liquid fuel cell by using formic acid as an anodic fuel and V^{4+} ions as a cathodic oxidant. The anodic formic acid decomposed into CO_2 and H_2O and the cathodic V^{4+} was reduced to $V^{3.5+}$. The valence state of electrolyte before and after the reaction was measured by using the UV-vis spectrum in Fig. 13(b), and there was only one characteristic absorption peak of V^{4+} at 760 nm, while an additional absorption peak of V^{3+} appeared at 610 nm after the reaction, which indicated that the fuel cell could achieve V^{4+} reduction. The reaction mode of the fuel cell opens a new pathway for the preparation of $V^{3.5+}$ electrolyte.

The selection of catalysts and reducing agents in catalytic reduction methods is extremely crucial. In addition to formic acid, ascorbic acid, oxalic acid and other available organic

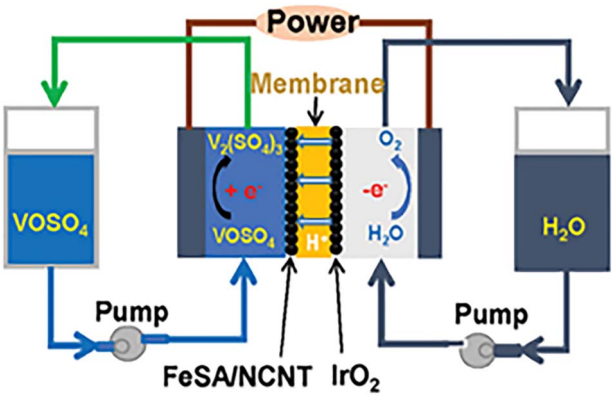

Fig. 15 Schematic of oxygen evolution electrolysis[73] (reprinted with permission from John Wiley and Sons).

reductants, the key is to find reductants with clean products, strong reducing ability, low cost and more applicability. The use of a platinum catalyst increases the production cost of the electrolyte, and there has not yet appeared a product that can replace the Pt/C catalyst, so it is necessary to develop new catalysts that can both improve the catalytic reaction speed and reduce the amount of platinum. Studies have been carried out to improve the durability and high efficiency of catalytic materials by means of improving Pt/C catalysts, such as doping metal elements, adjusting the electronic structure between materials, *etc.* The performance of the improved catalysts has been improved to a certain extent, and there are also some problems in practical applications.

3.2 Electrolysis method

3.2.1 Oxygen evolution electrolysis. Oxygen evolution electrolysis usually employs an electro-stack and its structure is[70] shown in Fig. 14. The electrolysis system is designed with a continuous-flow electro-stack structure with a perfluorosulfonic acid membrane as the separator, graphite plates as cathodes, and titanium plates or titanium-based coated electrodes as anodes; ruthenium–iridium (Ru–Ir) and iridium–tantalum (Ta–Ir) coatings exhibit excellent electrocatalytic activity and superior corrosion resistance. During the electrolysis process, a V_2O_5 sulfuric acid solution or $VOSO_4$ solution is introduced into the cathode, and V^{5+} or V^{4+} is reduced as shown in eqn (11) and (12). A sulfuric acid aqueous solution is electrolyzed with oxygen being generated at the anode as shown in eqn (13).[71] The electrochemical reaction and ion migration occurred in the battery driven by external electric energy, and finally the electric energy was converted into chemical energy for storage, as shown in Fig. 15. The anode produces O_2 and H^+, which drives the cathode to reduce V^{5+}/V^{4+} to $V^{3.5+}/V^{3+}$, and H^+ migrates through the membrane to complete the current loop. The reaction of the whole process is shown in eqn (14) and (15).

Cathode:

$$VO_2^+ + e^- + 2H^+ \rightarrow VO^{2+} + H_2O \quad (11)$$

$$VO^{2+} + e^- + 2H^+ \rightarrow V^{3+} + H_2O \quad (12)$$

Anode:

$$2H_2O - 4e^- \rightarrow 4H^+ + O_2\uparrow \quad (13)$$

Overall:

$$V_2O_5 + 3H_2SO_4 \rightarrow V_2(SO_4)_3 + 3H_2O + O_2\uparrow \quad (14)$$

$$4VOSO_4 + 2H_2SO_4 \rightarrow 2V_2(SO_4)_3 + 2H_2O + O_2\uparrow \quad (15)$$

As shown in Fig. 16, high-purity V_2O_5 powder, 4 to 5 mol per L sulfuric acid solution, and water are fed into the reaction vessel in specific proportions, under stirring and heating conditions to form an acidic slurry.[72] This slurry is then passed through a filtration unit to remove undissolved particles and impurities, yielding a clear solution. This solution undergoes a reduction reaction at the cathode of the electrolysis cell, and the resulting V^{3+} ions are circulated back to the reaction vessel. As indicated in eqn (8), V^{3+} acts as a chemical reducing agent that significantly accelerates the dissolution of V_2O_5, thereby mitigating its poor solubility. This method requires high-purity raw materials, and impurities may contaminate the electrolyte. Additionally, the highly acidic environment necessitates corrosion protection measures for the equipment.

The modular design of the stack structure by oxygen evolution electrolysis can highlight the integration advantages and allow it to operate at relatively high voltage, which is conducive

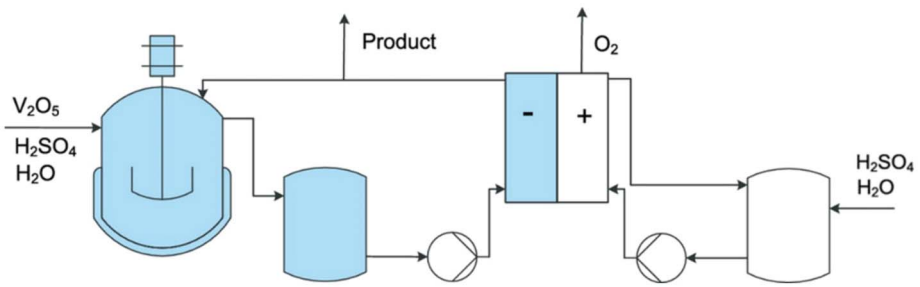

Fig. 16 Process flow for production of vanadium electrolyte[72] (reprinted with permission from John Wiley and Sons).

Table 3 Comparison of the oxygen evolution electrolysis and VFB electrolysis method

	Oxygen evolution electrolysis	VFB electrolysis
Anode material	Ti plate with Ru–Ir or Ir–Ta coatings	C-based substrates
Voltage	About 5 V	1–1.6 V
Anode electrolyte	H_2SO_4 solution	V^{4+} electrolyte
Cathode electrolyte	V^{5+}/V^{4+} electrolyte	V^{4+} electrolyte
Anode reaction	$H_2O \rightarrow O_2$	$V^{4+} \rightarrow V^{4.5+}$
Cathode reaction	$V^{5+}/V^{4+} \rightarrow V^{3.5+}$	$V^{4+} \rightarrow V^{3.5+}$

to shorten the reaction time, enhancing system adaptability and realizing large-scale continuous production.[74] Although the stack structure has brought the advantages of efficiency and adaptability, with strict equipment requirements and technical threshold, anode noble metal catalysts such as Ir and Ru are expensive and scarce, and the cost of corrosion-resistant materials and ion exchange membranes is also high. The initial investment for the whole electrolysis system is high, and the system needs to operate under the conditions of strong acidity and high potential, which puts forward extremely high requirements for the sealing, durability and daily maintenance of the equipment.

3.2.2 VFB electrolysis. The VFB electrolysis method involves injecting a V^{4+} electrolyte into the both the cathode and anode electrodes of VFBs, with the cathode electrode obtaining $V^{3.5+}$ or V^{3+}, whereas the anode electrode portion requires the addition of an additional reducing agent to lower the vanadium valence.[75] The reactions involved in the electrolysis–chemical reduction process are given in eqn (16)–(18), and the anode electrolyte usually needs to add an oxalate reducing agent to get V^{4+} by using eqn (19):

Cathode:

$$VO^{2+} + e^- + 2H^+ \rightarrow V^{3+} + H_2O \quad (16)$$

Anode:

$$VO^{2+} - e^- + H_2O \rightarrow VO_2^+ + 2H^+ \quad (17)$$

Overall:

$$2VO^{2+} \rightarrow VO_2^+ + V^{3+} \quad (18)$$

Chemical reduction:

$$VO_2^+ + C_2O_4^{2-} + 4H^+ \rightarrow 2CO_2 + VO^{2+} + 2H_2O \quad (19)$$

During the above process, the cathode and anode electrocatalytic electrodes are composed of one or more materials selected from C-based substrates. The C-based materials encompass graphitized/non-graphitized plates, porous carbon felt, carbon paper, or porous carbon plates, with pore diameters ranging between 1 and 200 μm. The battery electro-stack utilized in the VFB electrolysis method demonstrates significant structural and operational variations compared to the oxygen evolution electrolysis with detailed comparisons provided in Table 3.

The process of oxygen evolution electrolysis is short and it can consumes less time, and is commonly used in industry.[76,77] However, it requires high working voltage and high energy consumption, and relies on Ir/Ru-based noble metal catalysts. The acidic oxygen evolution reaction accelerates electrode corrosion, which affects the durability of equipment and increases the cost of long-term operation. The operating voltage and energy consumption of VFB electrolysis are low, and the electrolysis conditions are relatively mild. Carbon-based materials are mostly used, the system is simple and convenient to maintain and the relatively mild operating environment is conducive to long-term operation. However, the introduction of a reducing agent is complicated, which easily leads to a residue of impurities and affects the performance of electrolyte.

3.3 Chemical reduction–electrolysis method

The chemical reduction–electrolysis method is predominantly employed in industry, wherein V^{4+} electrolyte prepared from V^{5+} sources by chemical reduction necessitates supplementary electrolysis for the preparation of $V^{3.5+}$ electrolyte.[21,78]

3.3.1 Reduction of V_2O_5 in H_2SO_4 solution followed by electrolysis. At present, the commonly used method in industry is to reduce high-purity V_2O_5 (purity greater than 99.5%) with oxalic acid as the reducing agent to obtain sulfuric acid solution of $VOSO_4$. The resulting solution was incorporated into the VFB and charged through oxygen evolution electrolysis or VFB electrolysis to prepare $V^{3.5+}$ electrolyte. The reaction of reducing V_2O_5 to V^{4+} by using oxalic acid has the advantage of low temperature requirement and no need of high pressure. The heat of exothermic and redox reactions can be provided by diluting sulfuric acid to reach the temperature for a rapid and complete reaction. Yadong *et al.*[79] reduced V_2O_5 to prepare electrolytes utilizing reducing agents like oxalic acid, ascorbic acid, tartaric acid, citric acid, hydrogen peroxide, formic acid, and acetic acid. The preparation conditions of oxalic acid

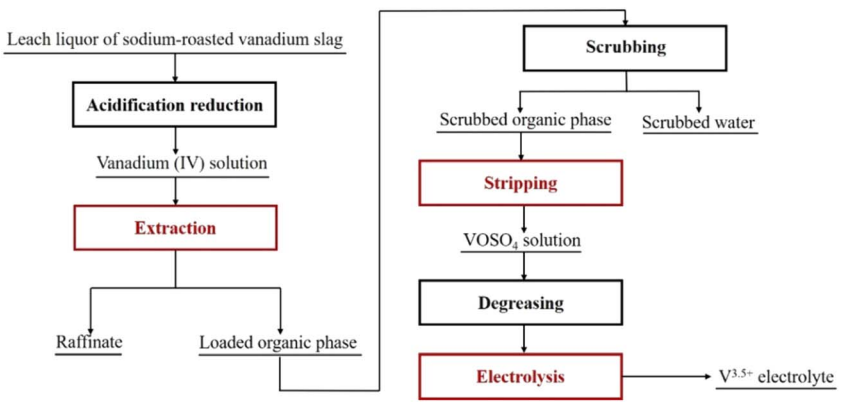

Fig. 17 Flow diagram for preparing $V^{3.5+}$ electrolyte by solvent extraction.

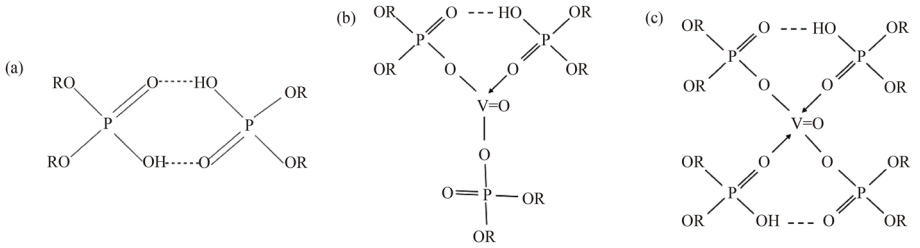

Fig. 18 (a) Dimer structure of the D2EHPA extractant in the organic phase; (b and c) VO^{2+} ions coordinate with multiple D2EHPA monomers in the loaded organic phase[84] (reprinted with permission from Springer Nature).

reduction to prepare electrolyte are a reaction temperature of 90 °C and reaction time of 100 min; the conversion rate of V^{5+} to V^{4+} reaches 94.8%.

The preparation of high-purity V_2O_5 is a key link because vanadium electrolyte has high requirements for impurity elements. In addition to using V_2O_5, related investigations[80] have adopted Na_3VO_4 solution as the raw material, the calcium vanadate solid was prepared by chemical precipitation, and V^{5+} was reduced to V^{4+} by using oxalic acid under strong acidic conditions to generate $VOSO_4$ solution. Calcium ions and sulfate ions formed calcium sulfate precipitation to remove it, and finally $V^{3.5+}$ electrolyte was obtained by electrolytic purification. This method uses the precipitation method to remove calcium ion impurities, which expands the selection range of raw materials, but the operation steps are complicated.

3.3.2 Solvent extraction of V(IV) followed by electrolysis. Due to the long preparation process, heavy pollution and low vanadium yield of high-purity V_2O_5 as the raw material,[81] the preparation cost of electrolyte is high. Therefore, purifying the intermediate or primary product of vanadium extraction in a metallurgical process to prepare vanadium electrolyte can shorten the process flow and reduce the production cost. The Institute of Process Engineering, Chinese Academy of Sciences, where the author is affiliated, put forward the method of extracting and purifying V^{4+} solution by solvent extraction to prepare $VOSO_4$ vanadium electrolyte[82] followed by electrolysis to prepare $V^{3.5+}$ electrolyte.

As shown in Fig. 17, the leach solution of sodium-roasted vanadium slag is used as the raw material, and sulfuric acid and a lower-priced reducing agent such as sodium sulfite are added to obtain crude tetravalent vanadium solution.[83] After extraction with the acidic phosphine extractant and scrubbing, V(IV) was selectively extracted, and impurities such as Cr, Al, Fe, Si, Ca, Cl and Na in the solution were effectively separated. After stripping with H_2SO_4 solution, the high-purity $VOSO_4$ electrolyte was obtained, which was treated by electrolysis to obtain $V^{3.5+}$ electrolyte. One kind of structure of the fresh extractant and vanadium-loaded extractant is shown in Fig. 18. The main reactions that occurred during the extraction process are represented as eqn (20) and (21).

$$VO_{(aq)}^{2+} + 2(HA)_{2(org)} \rightarrow VOA_2HA_{(org)} + 2H_{(aq)}^{+} + HA_{(org)} \quad (20)$$

$$VO_{(aq)}^{2+} + 2(HA)_{2(org)} \rightarrow VOA_2(HA)_{2(org)} + 2H_{(aq)}^{+} \quad (21)$$

The whole process of the method is based on a liquid–liquid reaction separation system, which simplifies the production

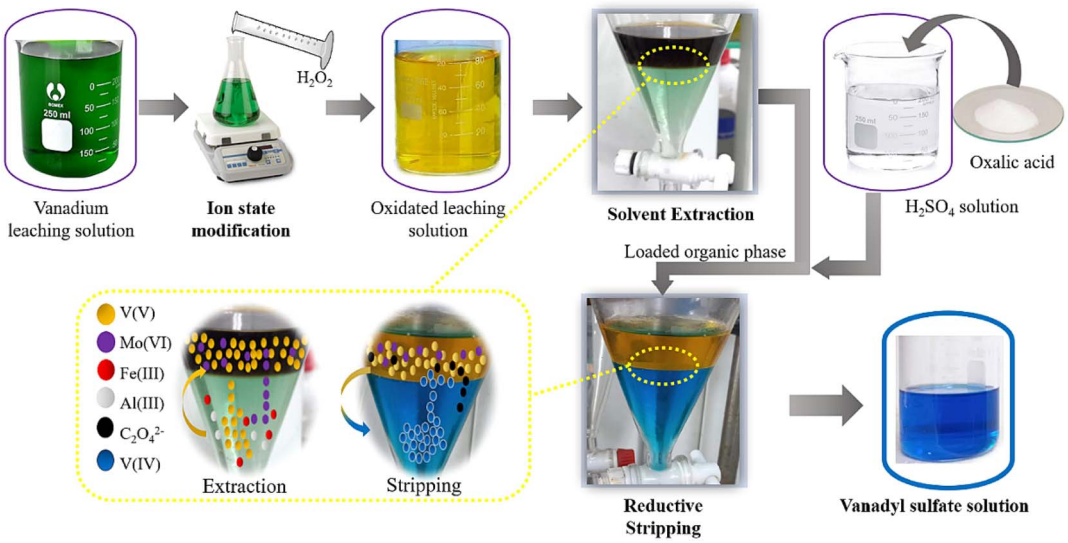

Fig. 19 Flow diagram of a solvent extraction–complexation reduction–stripping method[87] (reprinted with permission from Elsevier).

process, omits solid–liquid conversion processes such as preparation and dissolution of V_2O_5 in the traditional process, can get rid of dependence on high-purity vanadium raw materials, reduces the production cost, and has the advantages of shortening time and saving energy, and the extraction operation can realize continuous and automatic production with relatively high efficiency. Besides, the complexation between SO_4^{2-} and Cr(III) at higher SO_4 concentrations in this system inhibits the extraction of chromium, thus enhancing the separation of vanadium and chromium, and high-purity vanadium electrolyte with vanadium, chromium and sulfuric acid concentrations of 2.12 mol L^{-1}, 0.11 mg L^{-1} and 1.75 mol L^{-1} was prepared.[85] The prepared high-purity $VOSO_4$ electrolyte was de-oiled by resin or activated carbon, followed by further electrolysis to produce high-purity $V^{3.5+}$ electrolyte. At present, our research group has expanded the raw materials of this process to the leaching solution of stone coal, industrial crude ammonium metavanadate and ammonium poly-vanadate.

Up to now, solvent extraction of V(IV) with acidic phosphorus extractants such as P204 and P507 followed by electrolysis to prepare $V^{3.5+}$ electrolyte has become a research hotspot in this field. In recent related research, the raw solutions used in the extraction process involve vanadium slag calcified roasting reduction acid leaching solution,[86] stone coal acid leaching solution,[87] vanadium-rich solution after stone coal extraction and purification,[88] high chlorine stone coal leaching solution,[89] vanadium precipitation wastewater[90] and so on. Some improved methods involve using EDTA to complex ferric iron to inhibit iron extraction,[91] utilizing an H_2O_2–NaClO efficient selective oxidative stripping system within the D2EHPA extraction process, *etc.* Besides, the tri-octyl ammonium chloride (N263) extractant is also used in the preparation of vanadium electrolyte. With vanadium slag as the raw material, sodium diethyldithiocarbamate (DDTC) is used to complex V^{4+} ions in vanadium solution, which is recovered in the form of calcium salt CaV_2O_5, and then leached with carbonic acid and extracted with N263,[92] $VOSO_4$ electrolyte similar to commercial high-purity $VOSO_4$ is successfully prepared. Naseer, M. U. H. *et al.*[87] prepared vanadium sulfate electrolyte from the acid leaching solution of stone coal using a solvent extraction–complexation reduction–stripping method. As shown in Fig. 19, VO^{2+} ions are first oxidized by H_2O_2 form pentavalent $VO(O_2)_2^-$, followed by solvent extraction of vanadium using N263; an H_2SO_4 solution mixed with oxalic acid is used as the stripping solution, realizing the direct reduction and stripping of V^{5+} back to V^{4+}, ultimately yielding a $VOSO_4$ solution. The standard electrolyte sample (SS) was synthesized using a high-purity $VOSO_4$ crystal with both vanadium ion concentration and sulfuric acid concentration specifically the same as those for the electrolyte prepared through the solvent extraction methodology (ES).[90] As seen from the CV curve in Fig. 20(a) the anode peak current density (j_{pa}) obtained by SS is 84.18 mA cm^{-2} while that of ES is 77.91 mA cm^{-2}, and the j_{pa}/j_{pc} values are almost the same. The voltage change in the first charge–discharge cycle is shown in Fig. 20(b), the voltage efficiency (VE), energy efficiency (EE) and CE of ES and SS are shown in Fig. 20(c), in which CE and EE of ES are close to 90% of SS.

The above data show that the performance of electrolyte prepared by solvent extraction, and the charging and discharging characteristics are highly similar to those of the standard vanadium electrolyte, indicating that solvent extraction is a promising process. During the extraction process, trace amounts of oil at ppm levels inevitably contaminate the V^{4+} electrolyte due to solvent–solution contact. While the operational impact of such oil residues on VFBs remains undetermined, current purification techniques, utilizing resin or activated carbon adsorption to reduce oil content below 0.1 ppm, thereby mitigate potential adverse effects on VFB performance. How to improve the selectivity of the extractant and unoil the stripping liquid to avoid impurities from entering the product is a key problem that needs to be paid attention to in this method.

Compared with the single chemical reduction method and electrolysis method, chemical reduction–electrolysis technology is mature, and the process is more widely used. The addition of raw materials and reducing agents should be accurately controlled to ensure the purity and quality of electrolyte. The comprehensive application conditions of the two typical processes are shown in the following Table 4.

3.4 Sustainability analysis of preparation technology

Table 5 shows a comprehensive evaluation of the sustainable development ability of several typical methods, including the selection of raw materials, energy consumption, production of three wastes and economic principles. In the above process, the process parameters in the industry are estimated by combining

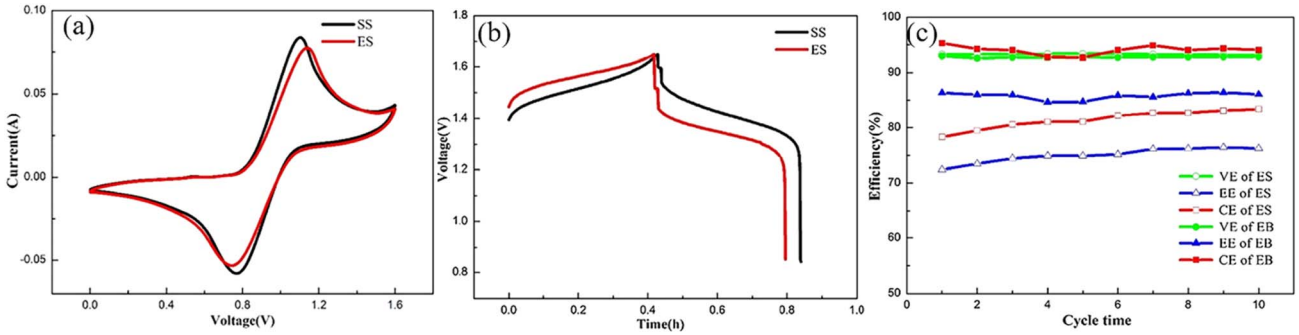

Fig. 20 (a) CV curves; (b) voltage change; (c) the efficiency of SS and ES[93] (reprinted with permission from Elsevier).

Table 4 Comprehensive comparison of two chemical reduction–electrolysis methods

	Reduction of V_2O_5 in H_2SO_4 solution	Solvent extraction of V(IV)
Raw material requirements	High-purity V_2O_5 (≥98%)	Vanadium leaching solution
Technological process	Dissolution → reduction → filtration → electrolysis	Pre-impurity removal → extraction → stripping → electrolysis
Cost of production	Long process, high energy consumption and high wastewater treatment cost	Short process and low energy consumption
Product purity	Readily residual oxalic acid impurities	The impurity content is low ($Na \leq 10$ mg L^{-1}, $Cr \leq 5$ mg L^{-1})
Technical maturity	Industrial application	Extensive industrial application demonstration stage
Environmental impact	Acid-containing wastewater and oxalic acid residue have high treatment cost	No ammonia nitrogen emission, recyclable solvent and clean production

with the general database, and the estimated electrolyte energy consumption of each comparative process is obtained for comparative analysis.[81]

For example, to calculate the energy consumption of preparing an electrolyte with a concentration of 1.6 mol per L $V^{3.5+}$ by oxalic acid reduction of V_2O_5 combined with electrolysis, the quantities of V_2O_5, $H_2C_2O_4$ and H_2SO_4 needed to produce 1 m^3 electrolyte are calculated according to the chemical reaction equation, and the energy consumption of raw material production is estimated by querying the database (LCA). According to the reaction equation, reducing 1.6 kmol of vanadium requires 0.8 kmol of oxalic acid, and the energy consumption for producing oxalic acid is about 25 MJ kg^{-1}, and the implied energy consumption is 1.80 GJ. The reactants are heated to the reaction temperature of 85 °C and maintained for several hours. According to the reaction temperature and holding time, the heat required for heating is calculated by using the average specific heat capacity of materials and the amount of materials used, and the total heat consumption is estimated by considering the energy consumption of electrolyte concentration and the heat loss efficiency of the reaction as shown in eqn (22). Assuming that the total mass of the system is about 1200 kg, mainly water and sulfuric acid, the average specific heat capacity C_P is about 4.0 kJ $(kg \cdot K)^{-1}$ and the thermal efficiency η is about 80%, the calculated sensible heat required for heating is about 7.5–9.0 GJ m^{-1}. The power and running time of the dasher, electrolytic equipment, *etc.* were estimated, and the amount of charge required to produce unit volume electrolyte was determined according to Faraday's law to calculate energy consumption. The theoretical charge Q required for reducing 0.8 kmol V^{4+} is calculated, the cell voltage is 0.5 V, the current efficiency is 90%, and the calculated power consumption is 35.74 kWh, which is converted into 0.129 GJ. The power consumption of pumps and control systems accounts for about 20% of the main power consumption, the total energy consumption of the electrolysis process is 0.155 GJ, and the total energy consumption is 10.455 GJ m^{-3}. The estimated range is 9–11 GJ.

$$E_{total} = E_{ele} + E_{th} + \sum(m_i \times EE_i) = \sum Pt + \sum cm\Delta t + \sum(m_i \times EE_i) \quad (22)$$

E_{total} represents the total energy consumption of the preparation process (GJ m^{-3}); E_{ele} represents the total power consumption in the preparation process (kWh); E_{th} represents the total heat consumption (GJ) during preparation; m_i represents the consumption mass of the chemical i (kg); EE_i represents the embodied energy (GJ kg^{-1}) of the chemical i.

4 Capacity recovery strategy of vanadium electrolyte

4.1 Capacity fading

During the long-term operation of VFBs, with the charge and discharge process, H^+ ions migrate at the anode and cathode. Due to the limited vanadium resistance of the ion exchange

Table 5 Evaluation of sustainable development ability of typical preparation methods of $V^{3.5+}$ electrolyte[81]

	Acid dissolution	Reduction roasting-acid dissolution	Electrolysis	Catalytic reduction	Chemical reduction–electrolysis
Raw material	V_2O_5/V_2O_3	V_2O_5/vanadate	$V_2O_5/VOSO_4$	$V_2O_5/VOSO_4$	Leaching solution/wastewater
Energy consumption	14–17 GJ m^{-3}	15–18 GJ m^{-3}	9–12 GJ m^{-3}	10–13 GJ m^{-3}	9–11 GJ m^{-3}
Three-wastes discharge	Acid waste water	Ammonia–nitrogen wastewater	Low hazardous waste	Catalyst residue treatment needed	CO_2 waste gas and solid waste
Economic viability	High-purity raw materials are difficult to obtain	Safety equipment for investment is high	Depends on the electricity price	Catalyst cost is high	The cost is relatively low

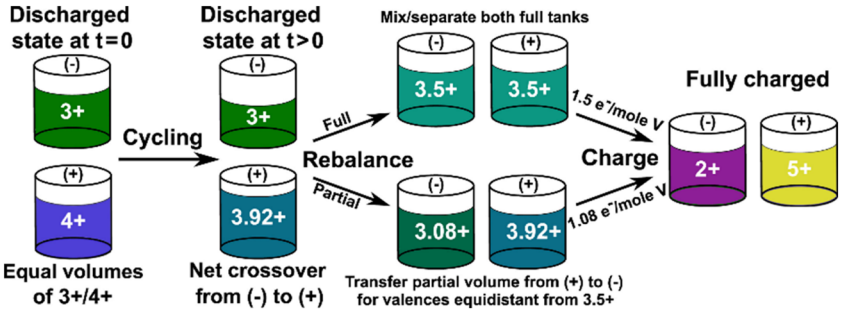

Fig. 21 Schematic of the full and partial rebalancing techniques[26] (reprinted with permission from Elsevier).

membrane, vanadium ions and water molecules will also migrate through the membrane under the action of an electric field and osmotic pressure.[94–96] For example, driven by the concentration gradient, V^{2+} ion migration occurs from the negative electrode through the ion exchange membrane to the positive electrode, resulting in a decrease in the volume of the negative electrode electrolyte and the total amount of vanadium ions, and the accumulation of vanadium ions in the positive electrode electrolyte, resulting in concentration imbalance. When V^{2+} migrates to the positive electrode, it will have a self-discharge reaction with high valence vanadium ions in the positive electrode, consuming electrons that can be used for normal charging and discharging, and making the average valence state of the electrolyte of the positive and negative electrodes deviate from 3.5 valence, and the valence state of the electrolyte is further unbalanced.[97]

In view of this capacity decay process, a related study[98] actively improves the initial average valence state of electrolyte and generates excessive VO_2^+ in the first charge–discharge cycle to inhibit the accumulation and migration of V^{2+} in the cycle process; however, this strategy will lead to a decrease in the actual available capacity in the first dozens of cycles, which really improves the stability and cumulative output capacity of the battery during the whole life cycle. The contact of oxygen in air with the negative electrolyte leads to an increase in the valence state of the electrolyte, and the occurrence of side reactions such as hydrogen evolution and oxygen evolution, which leads to the vanadium ions in the positive and negative electrolyte being mainly V^{5+} and V^{3+}, and the battery with unbalanced valence states between the positive and negative electrodes cannot be charged and discharged.[99–101] Most of the capacity loss can be recovered by mixing two kinds of half-cell electrolytes periodically, but the capacity loss caused by the hydrogen evolution reaction and air oxidation needs electrochemical or chemical rebalancing.[102] In addition to the above means of volume and valence recovery, there are also more studies on electrochemical system equipment, membrane

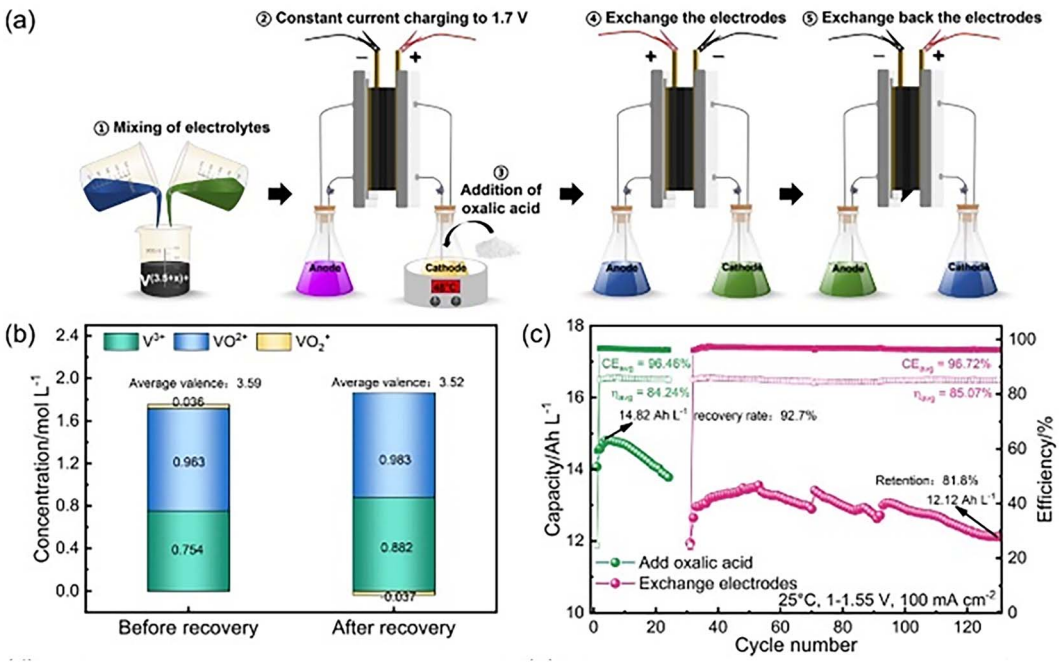

Fig. 22 (a) Schematic diagram; (b) comparison of electrolyte composition; (c) discharge specific capacity.[111]

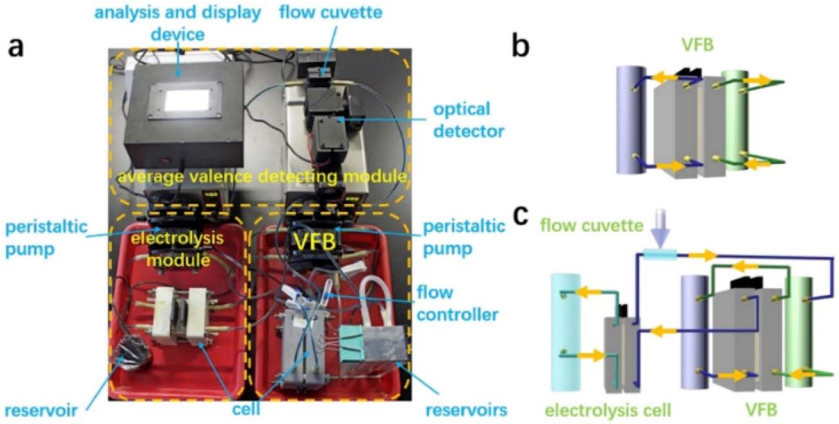

Fig. 23 (a) The photo capacity recovery system (b) in the normal mode and (c) in the recovery mode[114] (reprinted with permission from Elsevier).

improvement, *etc.*, dedicated to alleviating the decline in battery capacity from multiple perspectives.[103–105]

4.2 Capacity recovery

4.2.1 Positive and negative electrolyte mixing. The mixing of electrolytes can significantly extend the cycle life by restoring part of the capacity loss caused by the asymmetric transfer of various charged vanadium ions.[106] As shown in Fig. 21, when the volume deviation between the cathode and anode electrolytes reaches a certain extent, the electrolyte at the higher level is pumped by means of a transfer pump, an overflow pipe or a connecting pipe, to the electrolyte at the lower level to balance the concentration of vanadium ions in each electrolyte.[99,104]

4.2.2 Chemical reduction recovery. The chemical reduction recovery method of electrolyte includes the method of restoring battery capacity *in situ* by adding different reducing agents[107] as shown in Fig. 22(a), such as adding ammonium ferrous sulfate,[108] ascorbic acid, oxalic acid, formic acid and ethylene glycol to reduce anode V^{5+} electrolyte.[109,110] The equation when adding oxalic acid as then reducing agent is shown in eqn (23):

$$(VO_2)_2SO_4 + H_2C_2O_4 + H_2SO_4 \rightarrow 2VOSO_4 + 2H_2O + 2CO_2 \quad (23)$$

After the restoration with oxalic acid,[111] as can be seen from the discharge specific capacity curve in Fig. 22(b and c), the capacity decay of the battery significantly slows down after electrode exchange and restoration. After 130 cycles, the capacity retention rate is 81.8%, which is significantly higher than the retention rate of 64.2% after 100 cycles of the original pristine electrolyte. Meanwhile, the coulombic efficiency and energy efficiency of the battery significantly increase after electrode exchange and restoration, indicating a remarkable improvement in the electrochemical performance of the electrodes.

The addition of a chemical reducing agent to restore the valence state of the positive electrolyte mainly has the problems of imprecise control of the additive amount resulting in residuals, the introduction of impurities, and the need to avoid excessive reduction.

4.2.3 Electrolytic recovery. The electrolytic method employs an electrolytic cell structurally similarly to the battery configuration. Anodic water oxidation produces O_2, and the cathode reduces V^{5+} in the high-valence vanadium electrolyte with unbalanced valence state after long-term operation to lower oxidation states, thus restoring the average valence state of the electrolyte.[112,113] The VFB capacity recovery system is mainly composed of a VFB module and an electrolysis module connected by a pipeline and a flow controller as shown in Fig. 23(a). The positive electrolyte flows from the positive accumulator of the VFB through the positive cell, and then returns to the positive accumulator, and the same is true for the negative electrode in Fig. 23(b). The electrolyte flows through the negative storage tank, negative cell, positive storage tank and positive cell of the VFB, then flows through the negative cell of the electrolytic cell, and finally returns to the negative storage tank of the VFB, where the positive and negative electrode electrolytes are combined for in-line electrolysis to extend the cycle life of the VFB as shown in Fig. 23(c) This method reduces the average valence state of the mixed electrolyte through electrolysis, while incorporating real-time monitoring of valence state changes to ensure that the process reaches the optimal 3.5 valence endpoint. The use of electrolytic restoration can effectively restore the valence state without introducing impurities, but there is a problem that the electrolytic cell set is easily damaged due to untimely gas discharge and excessive pressure difference between the anode and cathode in high-power electrolysis.

5 Conclusions

This review provides a focused analysis of advanced methodologies for preparing $V^{3.5+}$ electrolytes. Comprehensive analysis including the chemical reduction method, electrolysis method, and chemical reduction–electrolysis method has been conducted. Their chemical principles, processes, advantages and limitations have been evaluated, while the preparation of high-purity $V^{3.5+}$ electrolyte still faces significant challenges.

Compared with high-purity $VOSO_4$ and V_2O_5, the selection of vanadium raw materials may have more possibilities. For example, extracting vanadium from vanadium-containing waste to prepare vanadium electrolyte has greater economic benefits and environmental value, and is also of great significance for the sustainable recycling of resources. At present, there is an urgent need for an efficient, stable and low-cost preparation route of $V^{3.5+}$ electrolyte, which can avoid introducing impurities to replace the conventional electrolysis method with high energy consumption and slow kinetics, and the reduction method with possible impurities and the high-cost noble metal catalysts. At the same time, no matter what kind of vanadium raw materials and preparation methods are used, VO_2^+ and VO^{2+} can be converted into $V^{3.5+}$ while ensuring the high purity of products, and the cycle life and cost of VFBs need to be considered to support their large-scale application in the production of industrial $V^{3.5+}$ electrolyte. The ideal preparation technology of vanadium electrolyte needs three dimensions: environmental friendliness, economic feasibility and the need of social sustainable development.

Author contributions

Pai Wang: investigation, writing – original draft. Fancheng Meng: conceptualization, methodology, writing – review & editing, project administration. Yu Qin: formal analysis, validation, writing – review & editing. Lina Wang: supervision, funding acquisition. Tao Qi: resources.

Conflicts of interest

The authors declare that they have no known competing financial interests or personal relationships that could have appeared to influence the work reported in this paper.

Data availability

This review article is based solely on previously published data (which can be found in the referenced articles), and no new data were generated.

Acknowledgements

The authors gratefully acknowledge the financial support from the Deep Earth Probe and Mineral Resources Exploration—National Science and Technology Major Project (2024ZD1003408) and Strategic Priority Research Program of the Chinese Academy of Sciences (XDA0430103).

References

1 K. C. Divya and J. Østergaard, *Elec. Power Syst. Res.*, 2009, **79**, 511–520.
2 X. Wang, Y. Zhang and H. Zhang, *J. Electrochem.*, 2015, **21**, 433–440.
3 B. Khaki and P. Das, *Electrochim. Acta*, 2022, **405**, 139842.
4 T.-N. Pham-Truong, Q. Wang, J. Ghilane and H. Randriamahazaka, *ChemSusChem*, 2020, **13**, 2142–2159.
5 M. Skyllas-Kazacos, G. Kazacos, G. Poon and H. Verseema, *Int. J. Energy Res.*, 2010, **34**, 182–189.
6 Z. Wei, A. Bhattarai, C. Zou, S. Meng, T. M. Lim and M. Skyllas-Kazacos, *J. Power Sources*, 2018, **390**, 261–269.
7 M. Kapoor, R. K. Gautam, V. K. Ramani and A. Verma, *Chem. Eng. J.*, 2020, **379**, 122300.
8 Y.-H. Fu, Y.-Y. Peng, L. Zhao, T.-Q. He, M.-M. Yuan, H. Dang, R. Liu and F. Ran, *Tungsten*, 2024, **6**, 561–573.
9 M. Rychcik and M. Skyllas-Kazacos, *J. Power Sources*, 1988, **22**, 59–67.
10 M. Skyllas-Kazacos, M. Rychcik, R. G. Robins, A. Fane and M. Green, *J. Electrochem. Soc.*, 1986, **133**, 1057.
11 J. Zhu, Y. Yuan and W. Wang, *Int. J. Electr. Power Energy Syst.*, 2019, **111**, 436–446.
12 M. U. H. Naseer, B. Pan, S. Wang, Y. Lyu, B. Liu, L. Li, J. Qi and H. Du, *J. Environ. Chem. Eng.*, 2025, **13**, 118402.
13 M. K. Singh, M. Kapoor and A. Verma, *Wiley Interdiscip. Rev. Energy Environ.*, 2021, **10**, e393.
14 C. Ding, H. Zhang, X. Li, T. Liu and F. Xing, *J. Phys. Chem. Lett.*, 2013, **4**, 1281–1294.
15 N. Beriwal and A. Verma, *Environ. Sci. Pollut. Res.*, 2022, **29**, 72187–72195.
16 H. Choi, D. Mandal and H. Kim, *ACS Sustain. Chem. Eng.*, 2022, **10**, 17143–17150.
17 J. Heo, J.-Y. Han, S. Kim, S. Yuk, C. Choi, R. Kim, J.-H. Lee, A. Klassen, S.-K. Ryi and H.-T. Kim, *Nat. Commun.*, 2019, **10**, 4412.
18 J. Noack, L. Wietschel, N. Roznyatovskaya, K. Pinkwart and J. Tübke, *Energies*, 2016, **9**, 627.
19 C. Minke, U. Kunz and T. Turek, *J. Power Sources*, 2017, **361**, 105–114.
20 G. Kear, A. A. Shah and F. C. Walsh, *Int. J. Energy Res.*, 2012, **36**, 1105–1120.
21 Y. Guo, J. Huang and J.-K. Feng, *J. Ind. Eng. Chem.*, 2023, **118**, 33–43.
22 X. Zang, L. Yan, Y. Yang, H. Pan, Z. Nie, K. W. Jung, Z. D. Deng and W. Wang, *Small Methods*, 2019, **3**, 1900494.
23 I. Rashitov, A. Voropay, G. Tsepilov, I. Kuzmin, A. Loskutov, A. Kurkin, E. Osetrov and I. Lipuzhin, *Batteries*, 2023, **9**, 464.
24 L. Wu, J. Wang, Y. Shen, L. Liu and J. Xi, *Phys. Chem. Chem. Phys.*, 2017, **19**, 14708–14717.
25 R. Pichugov, P. Loktionov, A. Pustovalova, A. Glazkov, A. Grishko, D. Konev, M. Petrov, A. Usenko and A. Antipov, *J. Power Sources*, 2023, **569**, 233013.
26 K. E. Rodby, T. J. Carney, Y. A. Gandomi, J. L. Barton, R. M. Darling and F. R. Brushett, *J. Power Sources*, 2020, **460**, 227958.
27 B. Khaki and P. Das, *Electrochim. Acta*, 2022, **405**, 139842.
28 L. Li, S. Kim, W. Wang, M. Vijayakumar, Z. Nie, B. Chen, J. Zhang, G. Xia, J. Hu and G. Graff, *Adv. Energy Mater.*, 2011, **1**, 394–400.
29 M. Zarei-Jelyani, M. M. Loghavi, M. Babaiee and R. Eqra, *J. Appl. Electrochem.*, 2024, **54**, 719–730.

30 N. Roznyatovskaya, J. Noack, H. Mild, M. Fühl, P. Fischer, K. Pinkwart, J. Tübke and M. Skyllas-Kazacos, *Batteries*, 2019, **5**, 13.
31 C. Fan, H. Yang and Q. Zhu, *Int. J. Electrochem. Sci.*, 2017, **12**, 7728–7738.
32 Y. Yang, Y. Zhang, L. Tang, T. Liu, J. Huang, S. Peng and X. Yang, *J. Power Sources*, 2019, **434**, 226719.
33 X. Wu, J. Liao, X. Yin, J. Liu, S. Wu, X. Wu, Z. Xie and W. Ling, *Chem. Commun.*, 2024, **60**, 2906–2909.
34 H.-J. Hong, H. S. Kim and Y. J. Suh, *Ind. Eng. Chem. Res.*, 2022, **61**, 11139–11147.
35 R. Aakesson, L. G. Pettersson, M. Sandstroem and U. Wahlgren, *J. Am. Chem. Soc.*, 1994, **116**, 8691–8704.
36 M. Benmelouka, S. Messaoudi, E. Furet, R. Gautier, E. Le Fur and J.-Y. Pivan, *J. Phys. Chem. A*, 2003, **107**, 4122–4129.
37 M. Vijayakumar, L. Li, Z. Nie, Z. Yang and J. Hu, *Phys. Chem. Chem. Phys.*, 2012, **14**, 10233–10242.
38 S. C. Larsen, *J. Phys. Chem. A*, 2001, **105**, 8333–8338.
39 C. V. Grant, W. Cope, J. A. Ball, G. G. Maresch, B. J. Gaffney, W. Fink and R. D. Britt, *J. Phys. Chem. B*, 1999, **103**, 10627–10631.
40 M. Vijayakumar, S. D. Burton, C. Huang, L. Li, Z. Yang, G. L. Graff, J. Liu, J. Hu and M. Skyllas-Kazacos, *J. Power Sources*, 2010, **195**, 7709–7717.
41 F. Sepehr and S. J. Paddison, *Chem. Phys. Lett.*, 2013, **585**, 53–58.
42 M. Bühl and M. Parrinello, *Chem.–Eur. J.*, 2001, **7**, 4487–4494.
43 J. Krakowiak, D. Lundberg and I. Persson, *Inorg. Chem.*, 2012, **51**, 9598–9609.
44 S. Gupta, N. Wai, T. M. Lim and S. H. Mushrif, *J. Mol. Liq.*, 2016, **215**, 596–602.
45 H. Peng, D. Tang, M. Liao, Y. Wu, X. Fan, B. Li, H. Huang and W. Shi, *Metals*, 2022, **12**, 557.
46 P. Hu, Y. Zhang, J. Huang, T. Liu, Y. Yuan and N. Xue, *ACS Sustain. Chem. Eng.*, 2018, **6**, 1900–1908.
47 X. Chen, J. Zhang and B. Yan, *Miner. Eng.*, 2021, **165**, 106864.
48 G. Park, Y. Lim, K. Hyun and Y. Kwon, *J. Power Sources*, 2024, **589**, 233770.
49 S. Das, S. Chakraborty, O. Parkash, D. Kumar, S. Bandyopadhyay, S. Samudrala, A. Sen and H. S. Maiti, *Talanta*, 2008, **75**, 385–389.
50 A. R. Petersen, L. B. Nielsen, J. R. Dethlefsen and P. Fristrup, *ChemCatChem*, 2018, **10**, 769–778.
51 K. Wang, Y. Zhang, L. Liu, J. Xi, Z. Wu and X. Qiu, *Electrochim. Acta*, 2018, **259**, 11–19.
52 S. Sun, L. Fang, H. Guo, L. Sun, Y. Liu and Y. J. S. Cheng, *Adv. Sci.*, 2023, **10**, 2207728.
53 W. Wang, X. Fan, J. Liu, C. Yan and C. Zeng, *J. Power Sources*, 2014, **261**, 212–220.
54 J. Xi, S. Xiao, L. Yu, L. Wu, L. Liu and X. Qiu, *Electrochim. Acta*, 2016, **191**, 695–704.
55 S. Xiao, L. Yu, L. Wu, L. Liu, X. Qiu and J. Xi, *Electrochim. Acta*, 2016, **187**, 525–534.
56 Y. Zeng, T. Zhao, L. An, X. Zhou and L. Wei, *J. Power Sources*, 2015, **300**, 438–443.
57 Z. Wang, Z. Qin, L. Chen, B. Liang, Y. Zhu, K. Wu and D. Luo, *Process Saf. Environ. Prot.*, 2023, **174**, 298–309.
58 D. He, Q. Feng, G. Zhang, L. Ou and Y. Lu, *Miner. Eng.*, 2007, **20**, 1184–1186.
59 R. Liu, J. Pan, X. Xie, S. Wang, J. Wang and T. Zhou, *J. Chem. Eng. Chin. Univ.*, 2014, **28**, 1275–1280.
60 X. Hui, Y. Xingrong and W. Xuewen, *Chinese Patent*, CN201711295760.X, 2022, 16.
61 N. Andriopoulos, C. E. Loo, R. Dukino and S. J. McGuire, *ISIJ Int.*, 2003, **43**, 1528–1537.
62 W. M. Carvalho, L. Cassayre, D. Quaranta, F. Chauvet, R. El-Hage, T. Tzedakis and B. Biscans, *J. Energy Chem.*, 2021, **61**, 436–445.
63 J. Martin, K. Schafner and T. T. Turek, *Energy Technol.*, 2020, **8**, 2000522.
64 W. Li, R. Zaffou, C. C. Sholvin, M. L. Perry and Y. She, *ECS Trans.*, 2013, **53**, 93.
65 Y. Hu, Y. Zhang, N. Xue and P. Hu, *Sep. Purif. Technol.*, 2024, **338**, 126496.
66 Z. Li, C. Wu and H. Wan, *Study on a Short Process Method for Preparation of 3.5 Valence Vanadium Electrolyte*, Springer International Publishing, 2022, pp. 470–478, DOI: **10.1007/978-3-030-92381-5_43**.
67 C. Wang, L.-J. Li and H. Du, *Tungsten*, 2024, **6**, 555–560.
68 C. Hu, Y. Dong, W. Zhang, H. Zhang, P. Zhou and H. Xu, *J. Power Sources*, 2023, **555**, 232330, DOI: **10.1016/J.JPOWSOUR.2022.232330.**
69 N. H. Choi, S.-k. Kwon and H. Kim, *J. Electrochem. Soc.*, 2013, **160**, A973.
70 A. A. Pustovalova, P. A. Loktionov, I. O. Speshilov, R. D. Pichugov, A. Y. Grishko, A. T. Glazkov and A. E. Antipov, *J. Power Sources*, 2023, **576**, 233211.
71 T. Sukkar and M. Skyllas-Kazacos, *J. Membr. Sci.*, 2003, **222**, 235–247.
72 J. Martin, K. Schafner and T. Turek, *Energy Technol.*, 2020, **8**, 2000522.
73 S. Niu, H. Li, H. Guo, Y. Liu and Y. Cheng, *Small*, 2024, **20**, 2405827.
74 E. B. Agyekum, M. Abdullah, F. Odoi-Yorke, A. Ameen, P. Chowdhury, M. A. Raza, F. L. Rashid and A. K. Hussein, *Energy Convers. Manage.:X*, 2025, **27**, 101180.
75 Y. Wen, Y. Xu and J. Cheng, *Chinese Patent*, CN201310542929.2, 2015, 6.
76 W. M. Carvalho Jr, L. Cassayre, D. Quaranta, F. Chauvet, R. El-Hage, T. Tzedakis and B. Biscans, *J. Energy Chem.*, 2021, **61**, 436–445.
77 Q. Aimiao, Q. Guo, C. Wang, A. Qin, X. J. Q. Chen, C. Wang, A. Qin and X. Chen, *SSRN Electron. J.*, 2022, DOI: **10.2139/ssrn.4015145**.
78 W. Tian, H. Du, J. Wang, J. J. Weigand, J. Qi, S. Wang and L. Li, *Materials*, 2023, **16**, 4582.
79 Y. Yadong, Z. Yimin, H. Jing, L. Tao and Z. Qiushi, *Chem. Ind. Eng. Prog.*, 2017, **36**, 274.
80 B. Liu, Y. Guo and X. Bi, *Chinese Patent*, CN202310512028.2, 2023, 8.
81 W. Gao, Z. Sun, H. Cao, H. Ding, Y. Zeng, P. Ning, G. Xu and Y. Zhang, *J. Clean. Prod.*, 2020, **256**, 120217.

82 D. Li, D. Chen and G. Zhang, *Metals*, 2017, **7**, 106, DOI: 10.3390/met7030106.
83 X. Zhang, F. Meng, Z. Zhu, D. Chen, H. Zhao, Y. Liu, Y. Zhen, T. Qi, S. Zheng and M. Wang, *Hydrometallurgy*, 2022, **208**, 105805.
84 H. Liu, Y.-M. Zhang, J. Huang and T. Liu, *Front. Chem. Sci. Eng.*, 2023, **17**, 56–67.
85 Y. Wang, Y. Liu, F. Meng, J. Zhang, S. Zhao, X. Tian, L. Wang, D. Chen and T. Qi, *Sep. Purif. Technol.*, 2025, **354**, 129281.
86 C. Li, T. Jiang, J. Wen, G. Yang, T. Yu, L. Zhang, X. An, G. Hao and X. Liu, *Chem. Eng. J.*, 2025, **511**, 162151.
87 M. U. H. Naseer, S. Wang, B. Liu, Y. Lyu, C. Bingxu, C. Wang, B. Pan and H. Du, *Sep. Purif. Technol.*, 2024, **340**, 126777.
88 Y.-W. Hu, Y.-M. Zhang, T. Liu and H. Liu, *J. Clean. Prod.*, 2023, **394**, 136389.
89 H. Liu, Y.-m. Zhang, T. Liu, J. Huang, L.-m. Chen and Y.-w. Hu, *Trans. Nonferrous Metals Soc. China*, 2023, **33**, 1594–1608.
90 C. Liu, T. Liu, Y. Zhang, Z. Dai and Y. Yang, *Sep. Purif. Technol.*, 2020, **240**, 116582.
91 Y. Zhang, D. Dreisinger, T.-A. Zhang, G. Lv, W. Zhang and F. Xie, *Hydrometallurgy*, 2019, **188**, 54–63.
92 Z. Wang, L. Chen, R. Yin, Z. Li, G. Deng, B. Liang, Y. Zhu, K. Wu and D. Luo, *Hydrometallurgy*, 2023, **222**, 106146.
93 M. U. H. Naseer, S. Wang, B. Liu, Y. Lyu, C. Bingxu, C. Wang, B. Pan and H. Du, *Sep. Purif. Technol.*, 2024, **340**, 126777.
94 N. Blume, O. Zielinski, M. Becker and C. Minke, *Energy Technol.*, 2024, **12**, 2300750.
95 M. Kapoor, N. Beriwal and A. Verma, *J. Energy Storage*, 2020, **32**, 101759.
96 M. Skyllas-Kazacos and L. Goh, *J. Membr. Sci.*, 2012, **399**, 43–48.
97 Y. Wang, A. Mu, W. Wang, B. Yang and J. Wang, *ChemSusChem*, 2024, **17**, e202301787.
98 Z. Wang, Z. Guo, J. Ren, Y. Li, B. Liu, X. Fan and T. Zhao, *ACS Cent. Sci.*, 2023, **9**, 56–63.
99 K. Oh, S. Won and H. Ju, *Electrochim. Acta*, 2015, **181**, 238–247.
100 C. Sun, J. Chen, H. Zhang, X. Han and Q. Luo, *J. Power Sources*, 2010, **195**, 890–897.
101 Q. Luo, L. Li, W. Wang, Z. Nie, X. Wei, B. Li, B. Chen, Z. Yang and V. Sprenkle, *ChemSusChem*, 2013, **6**, 268–274.
102 C. Choi, S. Kim, R. Kim, Y. Choi, S. Kim, H.-y. Jung, J. H. Yang and H.-T. Kim, *Renew. Sustain. Energy Rev.*, 2017, **69**, 263–274.
103 X.-G. Yang, Q. Ye, P. Cheng and T. S. Zhao, *Appl. Energy*, 2015, **145**, 306–319.
104 Y. Zhang, L. Liu, J. Xi, Z. Wu and X. Qiu, *Appl. Energy*, 2017, **204**, 373–381.
105 R. M. Darling, A. Z. Weber, M. C. Tucker and M. L. Perry, *J. Electrochem. Soc.*, 2015, **163**, A5014.
106 K. Wang, L. Liu, J. Xi, Z. Wu and X. Qiu, *J. Power Sources*, 2017, **338**, 17–25.
107 L. Wei, X. Fan, H. Jiang, K. Liu, M. Wu and T. Zhao, *J. Power Sources*, 2020, **478**, 228725.
108 D. Shi, H. Zhang and X. Li, *Chinese Patent*, CN201510927447.8, 2020, 6.
109 P. Loktionov, R. Pichugov, D. Konev and A. Antipov, *Electrochim. Acta*, 2022, **436**, 141451.
110 Z. Zhao, H. C. Liu and Q. Ge, *Chinese Patent*, CN202310659813.0, 2023, 11.
111 Y. Tao, W. Yijun and T. Zilong, *Energy Storage Sci. Technol.*, 2025, **14**, 1177–1186, DOI: 10.19799/j.cnki.2095-4239.2024.0838.
112 J. Chen, H. Zhang and C. Sun, *Chinese Patent*, CN200810012119.5, 2010, 24.
113 Z. Li, J. Xi, L. Liu, Z. Wu and D. Li, *ACS Sustain. Chem. Eng.*, 2020, **8**, 10275–10283.
114 R. Gundlapalli and S. Jayanti, *J. Energy Storage*, 2019, **23**, 148.